




MOV10 recruits DCP2 to decap human LINE-1 RNA by forming large cytoplasmic granules with phase separation properties

Qian Liu^{1,†}, Dongrong Yi^{1,†}, Jiwei Ding¹, Yang Mao¹, Shujie Wang¹, Ling Ma¹, Quanjie Li¹, Jing Wang¹, Yongxin Zhang¹, Jianyuan Zhao¹, Saisai Guo¹, Zhenlong Liu² , Fei Guo³ , Dongbing Zhao^{4,*}, Chen Liang², Xiaoyu Li^{1,**}, Xiaozhong Peng^{5,***} & Shan Cen^{1,****} 

Abstract

Long interspersed element 1 (LINE-1) is the only active autonomous mobile element in the human genome. Its transposition can exert deleterious effects on the structure and function of the host genome and cause sporadic genetic diseases. Tight control of LINE-1 mobilization by the host is crucial for genetic stability. In this study, we report that MOV10 recruits the main decapping enzyme DCP2 to LINE-1 RNA and forms a complex of MOV10, DCP2, and LINE-1 RNP, exhibiting liquid–liquid phase separation (LLPS) properties. DCP2 cooperates with MOV10 to decap LINE-1 RNA, which causes degradation of LINE-1 RNA and thus reduces LINE-1 retrotransposition. We here identify DCP2 as one of the key effector proteins determining LINE-1 replication, and elucidate an LLPS mechanism that facilitates the anti-LINE-1 action of MOV10 and DCP2.

Keywords DCP2; LINE-1; liquid–liquid phase separation; MOV10; RNA decap

Subject Categories Chromatin, Transcription & Genomics; DNA Replication, Recombination & Repair; RNA Biology

DOI 10.15252/embr.202256512 | Received 19 November 2022 | Revised 22 June 2023 | Accepted 28 June 2023 | Published online 12 July 2023

EMBO Reports (2023) 24: e56512

Introduction

Long interspersed elements (LINEs) are a group of active non-long-terminal repeat (LTR) retrotransposons, comprising approximately 17% of the human genome (reviewed in Goodier & Kazazian, 2008).

Full-length human long interspersed element 1 (LINE-1) is ~ 6,000 nucleotides in length and has three open reading frames: ORF1, ORF2, and ORF0. ORF1p engages in nucleic acid binding and nucleic acid chaperone activities (2–6). ORF2p engages in two types of enzymatic activity: single-strand endonuclease (Feng *et al*, 1996) and reverse transcriptase (Dombroski *et al*, 1994). ORF1p and ORF2p bind to LINE-1 RNA in a cis-acting manner to form RNA protein complexes (RNP). Once the RNP translocates into the nucleus, LINE-1 RNA is reverse-transcribed and inserted into cellular DNA via target-site priming reverse transcription (TPRT; Luan *et al*, 1993; Feng *et al*, 1996; Cost *et al*, 2002). The third ORF, ORF0, is expressed from an antisense promoter in the 5' untranslated (UTR) of LINE-1, and influences the retrotransposition process. However, the exact function of ORF0 is still unknown (Denli *et al*, 2015). Although most LINE-1 elements in the human genome are retrotransposition-deficient due to 5' truncation, internal deletions, or other mutations, there are still ~ 80–100 full-length active LINE-1 elements (Brouha *et al*, 2003; Beck *et al*, 2010), causing the insertion, deletion, and recombination of host DNA (Gilbert *et al*, 2002; Han *et al*, 2004; Gasior *et al*, 2006; Belancio *et al*, 2008; Iskow *et al*, 2010). Furthermore, LINE-1 proteins also support the retrotransposition of short interspersed elements, including Alu and SVA, which do not encode their own proteins (Lander *et al*, 2001). The actions of LINE-1, Alu, and SVA are the causes of many genetic diseases (Goodier, 2016). Additionally, recent evidence suggests that LINE-1 activity contributes to age-related diseases and that LINE-1-derived nucleic acids can trigger inflammatory responses (Chen *et al*, 2020).

Given the potential harm that LINE-1 may cause, host cells have evolved multiple mechanisms to control LINE-1 replication at transcriptional and post-transcriptional levels (reviewed in

1 Institute of Medicinal Biotechnology, Chinese Academy of Medical Sciences and Peking Union Medical School, Beijing, China

2 Lady Davis Institute, Jewish General Hospital, McGill University, Montreal, QC, Canada

3 Institute of Pathogen Biology, Chinese Academy of Medical Science, Beijing, China

4 National Cancer Center, Chinese Academy of Medical Sciences and Peking Union Medical School, Beijing, China

5 State Key Laboratory of Medical Molecular Biology, Department of Molecular Biology and Biochemistry, Institute of Basic Medical Sciences, Medical Primate Research Center, Neuroscience Center, Chinese Academy of Medical Sciences, School of Basic Medicine Peking Union Medical College, Beijing, China

*Corresponding author. Tel: +86 10 63037279; Fax: +86 10 63037279; E-mail: shancen@imb.pumc.edu.cn

**Corresponding author. Tel: +86 10 63131011; Fax: +86 010 63037279; E-mail: lixiaoyu@imb.pumc.edu.cn

***Corresponding author. Tel: +86 10 67779915; E-mail: pengxiaozhong@pumc.edu.cn

****Corresponding author. Tel: +86 13901331816; E-mail: dbzhao@cicams.ac

†These authors contributed equally to this work as first authors

Goodier, 2016). Recent studies have revealed the roles of innate restriction factors, such as APOBEC3 proteins and SAMHD1, and the RNA helicase MOV10 (Chen *et al*, 2006; Muckenfuss *et al*, 2006; Stenglein & Harris, 2006; Kinomoto *et al*, 2007; MacDuff *et al*, 2009; Tan *et al*, 2009; Arjan-Odedra *et al*, 2012; Goodier *et al*, 2012, 2015; Li *et al*, 2013; Richardson *et al*, 2014; Moldovan & Moran, 2015; Hu *et al*, 2015b; Liang *et al*, 2016; Warkocki *et al*, 2018). MOV10 is a putative member of the SF1 family helicases (Chen *et al*, 2020) and was first identified by provirus integration in the Moloney leukemia virus type 10 mouse strain as an ATP-binding protein (Mooslehner *et al*, 1991). It has RNA binding properties and 5' to 3' RNA duplex unwinding activity (Gregersen *et al*, 2014). In addition to restricting a range of RNA viruses and retroviruses (Haussecker *et al*, 2008; Burdick *et al*, 2010; Furtak *et al*, 2010; Wang *et al*, 2010, 2016; Schoggins *et al*, 2011; Zhang *et al*, 2016; Balinsky *et al*, 2017; Puray-Chavez *et al*, 2019), MOV10 also inhibits retroelements including LINE-1, through cooperation with several host factors such as UPF1 and RNASEH2 (Arjan-Odedra *et al*, 2012; Goodier *et al*, 2012; Lu *et al*, 2012; Li *et al*, 2013; Gregersen *et al*, 2014; Skariah *et al*, 2017; Choi *et al*, 2018; Warkocki *et al*, 2018). However, the detailed mechanisms remain elusive. We previously reported that MOV10 induces degradation of LINE-1 RNA (Li *et al*, 2013), suggesting that MOV10 may utilize the mRNA decay machinery to degrade LINE-1 RNA.

The 5' 7-methylguanosine cap and the 3' poly(A) tail protect eukaryotic RNA from degradation by the mRNA decay machinery. Decay of most mRNA species begins by a reversible poly(A) tail-shortening step, and the mRNA bearing the correct signals can be readenylated. Once RNA transcripts are destined for degradation, they follow one of two irreversible pathways. One pathway requires the removal of the 5' cap by DCP2, and the decapped mRNA is degraded in the 5' to 3' direction by the XRN1 exoribonuclease. In another pathway, the 3'-end deadenylated mRNA is degraded by a large 3' to 5' exonuclease complex, known as the exosome (reviewed in Garneau *et al*, 2007).

In this study, we provide evidence supporting the mechanism that MOV10 causes degradation of LINE-1 RNA by engaging in the DCP2-dependent RNA decay pathway. Specifically, MOV10 interacts with DCP2 and forms a DCP2/MOV10/LINE-1 RNP complex that is driven by liquid-liquid phase separation, thereby leading to the degradation of LINE-1 RNA and the inhibition of LINE-1 retrotransposition.

Results

DCP2 interacts with MOV10

To understand the detailed mechanism underlying MOV10-mediated restriction of LINE-1 retrotransposition, we first performed immunoprecipitation coupled with a mass spectrometry (MS) approach to identify cellular proteins associated with MOV10. Briefly, Flag-tagged MOV10 was expressed in HEK293T cells and then immunoprecipitated with a IgG antibody (Dataset EV1 and EV3) or a Flag-specific antibody (Dataset EV2 and EV4) or, followed by MS analysis of the immunoprecipitated materials. The data from two independent experiments was collected. The results highlighted 307 MOV10-associated proteins (Fig 1A) that were present only (Fig 1B) or significantly increased (> 2-fold) (Fig 1C) in the anti-Flag samples. Among these factors, UPF1 and PABPC4 were previously reported to associate with MOV10 (Gregersen *et al*, 2014). Gene ontology (GO) analysis showed that 56% of these proteins were enriched in mRNA catabolic processes and nonsense-mediated decay, and 11% were enriched in the regulation of RNA stability (Fig 1C). Kyoto Encyclopedia of Genes and Genomes (KEGG) analysis showed that four of these proteins were involved in the RNA degradation pathway (Fig 1D and E).

It is known that DCP2 functions as the main eukaryotic decapping enzyme to remove the 5' cap of mRNA and trigger mRNA degradation. The association of DCP2 with the ectopically expressed Flag-tagged MOV10 (Fig 1F) or endogenous MOV10 (Fig 1G) was confirmed by the results of co-immunoprecipitation (co-IP) as well as by the data of immunofluorescence staining showing the strong colocalization of MOV10 and DCP2 (Fig 1H). Since both MOV10 and DCP2 have been shown to localize in the P-body, we further probed MOV10-immunoprecipitated samples for the presence of P-body marker proteins, including LSM1, RCK, and EDC3, and none were detected (Fig EV1). This further supports the specificity of the interaction between DCP2 and MOV10. This suggests that the interaction between DCP2 and MOV10 is not resulted from their colocalization in P-body.

Several lines of evidence have shown that two exonucleases, CCR4 and XRN1, are involved in DCP2-mediated RNA decay, which degrade RNA in two opposite directions (Garneau *et al*, 2007). However, neither XRN1 nor CCR4 was found to be associated with MOV10, as shown by the data from the co-IP experiments (Fig 1D). DCP2 has also been reported to interact with the decapping activator

Figure 1. MOV10 interacts with DCP2.

- Venn diagram showing overlaps of enriched proteins between the two extraction conditions.
- Scattergram showing the 173 proteins present in anti-Flag sample only sorted by intensity.
- Heatmap presenting the 134 proteins present in Flag-MOV10 sample only increase significantly (>2 fold).
- GO enrichment analysis of MOV10-immunoprecipitated proteins. The bars indicate the number of proteins in each GO category. BP represents biological process. CC represents cellular component. MF represents molecular function.
- Kyoto Encyclopedia of Genes and Genomes (KEGG) analysis shows the involvement of MOV10-immunoprecipitated proteins in RNA degradation pathway.
- Immunoblotting analysis of MOV10, CCR4, XRN1, and DCP2 from co-IPs. HEK293T cells were transiently transfected with Flag-MOV10 expressing plasmid and CMV-L1-neo^{RT}. Input and anti-Flag IPs were subjected to immunoblot analysis using antibodies against CCR4, XRN1, and DCP2, and actin was used as loading control (*n* = 3 biological replicates).
- Immunoprecipitation of endogenous MOV10 protein in HEK293T cells with or without RNase treatment. The IPs were subjected to immunoblot using antibodies against MOV10 and DCP2.
- Confocal microscopy showing cytoplasmic localization of Flag-MOV10 (green) and DCP2 (red) (*n* = 3 biological replicates).

Source data are available online for this figure.

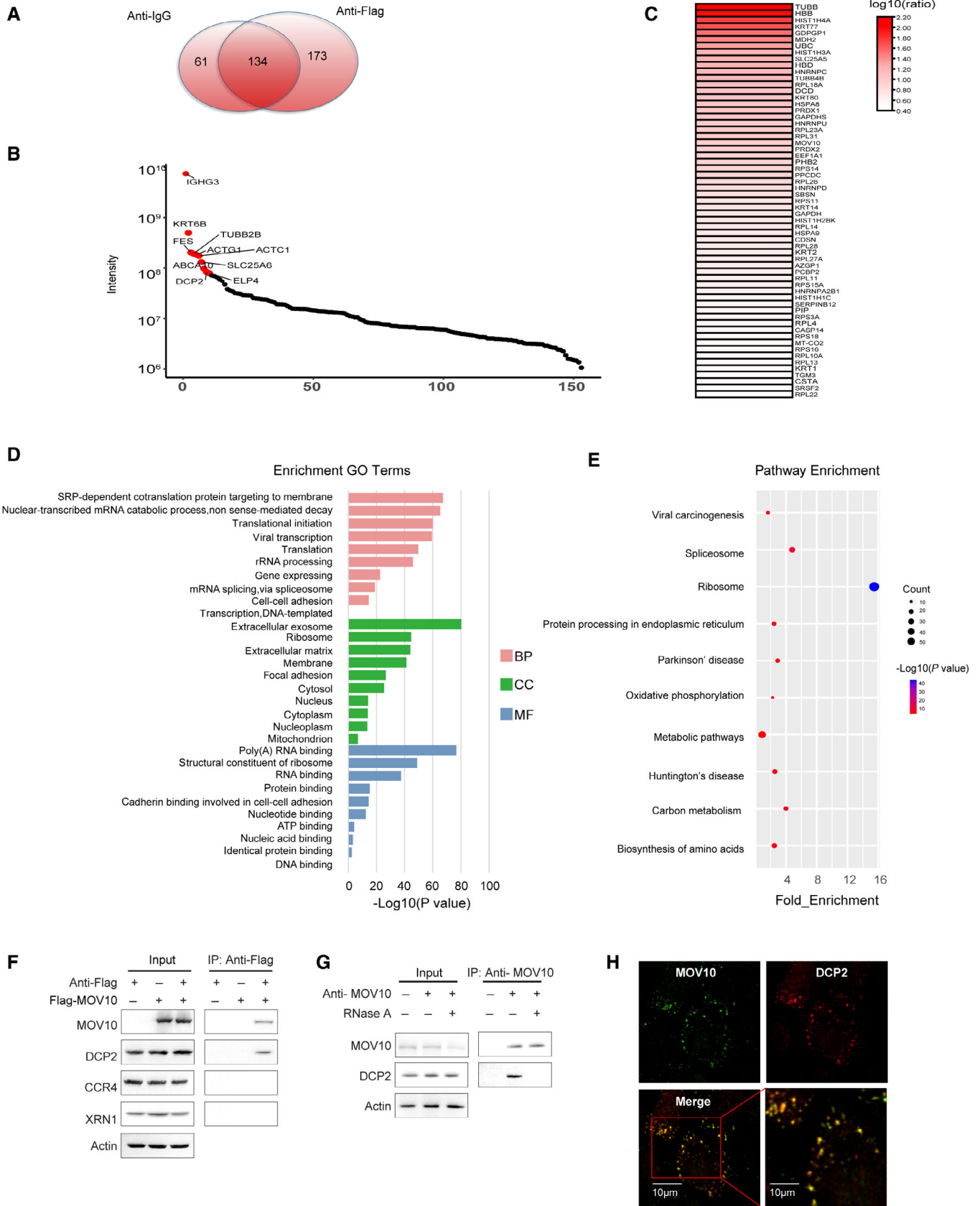


Figure 1.

DCP1, which enhances the decapping activity of DCP2 (Garneau *et al*, 2007).

DCP2 cooperates with MOV10 in the degradation of LINE-1 RNA and the inhibition of LINE-1 retrotransposition

Next, we investigated whether DCP2 plays a role in MOV10-mediated restriction of LINE-1 replication using a CMV-L1-neo^{RT} reporter as previously described (Li *et al*, 2013). In the CMV-L1-neo^{RT} reporter construct, a neomycin resistance gene containing an intron sequence was inserted between ORF2p and the 3'UTR of LINE-1 in the opposite direction (Esnault *et al*, 2000); thus, the neomycin gene can only be expressed upon successful reverse transcription of LINE-1 RNA, which can be determined by scoring G418-resistant cell colonies (Fig EV2A). HeLa cells were cotransfected with CMV-L1-neo^{RT} and increasing amounts of plasmids expressing DCP2, followed by quantification of LINE-1 RNA by RT-qPCR and the LINE-1 retrotransposition assay. To quantify LINE-1 RNA, a pair of primers are designed to target to neo gene span the Neo cassette intron of the transfected L1 construct such that only LINE-1 cDNA that has been reverse transcribed from the spliced RNA is amplified. We found that with increasing expression of DCP2, the LINE-1 RNA level gradually decreased to 50% ($P < 0.05$) in a dose-dependent manner (Fig 2A), accompanied by a similar reduction in the number of G418-resistant HeLa cell colonies (Fig 2B). A similar reduction in LINE-1 RNA was observed using another pair of primers targeting on LINE-1 5'UTR (Fig EV2E). These data suggest that DCP2 has the ability to restrict LINE-1 retrotransposition through reducing LINE-1 RNA expression.

We then co-expressed exogenous MOV10 and DCP2, and observed greater inhibition of LINE-1 RNA expression (Fig 2A) and LINE-1 retrotransposition (Fig 2B) than when either MOV10 or DCP2 are expressed alone, which indicates a cooperative action of MOV10 and DCP2 in restricting LINE-1. When endogenous *MOV10* was knocked down with short interfering RNA (siRNA), overexpression of DCP2 no longer significantly affected the expression of LINE-1 RNA or the number of G418-resistant cell colonies (Fig 2C and D). Similarly, when endogenous DCP2 in HeLa cells was depleted with siRNA, the inhibitory activity of MOV10 against LINE-1 RNA or LINE-1 retrotransposition were also dramatically impaired (Fig 2E and F). A similar reduction in LINE-1 RNA was observed using another pair of primers targeting on LINE-1 5'UTR (Fig EV2F and G).

It should be noted that in the CMV-L1-neoRT reporter, the native LINE-1 promoter is supplemented by an adjacent CMV promoter. Therefore, it is possible that the effect of DCP2 upon LINE-1 retrotransposition efficiency may be at least in part due to the presence of the CMV promoter sequence. To address this, we have performed the retrotransposition assays using a plasmid L1-neoRT, which only contains the native LINE-1 promoter without the adjacent CMV promoter. In addition, CMV-L1-neoRT (D702Y), a mutant has the 702 amino acids Asp mutated to Tyr, are inactivated to form colonies and included as a control. As shown in the Fig EV2H and I, the similar inhibitory effect of MOV10 and DCP2 on retrotransposition of both LINE-1 reporters suggests that the CMV promoter sequence shall have a very limited effect on the impact that DCP2 has on LINE-1 retrotransposition efficiency.

In addition to HeLa cells, we also measured the effect of DCP2 and MOV10 on the activity of LINE-1 in HEK293T cells, and found

marked reduction in LINE-1 RNA expression and LINE-1 retrotransposition by these two proteins (Fig EV2B–D). Together, these data indicate that MOV10 and DCP2 work together as one functional complex to restrict LINE-1 retrotransposition.

Since DCP2 involves in mRNA metabolism and shall be a general important factor to cell proliferation, its overexpression or knockdown may affect cell viability and thereby result in a bias in the retrotransposition assay. To address this, the viability of HeLa cells with DCP2 or MOV10 overexpression or knockdown were assessed, and modest reduction in the cell viabilities were observed compared with control cells (Fig EV2J and K), suggesting minor effect of these transient treatment on cell proliferation.

DCP2 decaps LINE-1 RNA in a MOV10-dependent manner

DCP2-mediated removal of the 5' cap initiates irreversible decay of the mRNA. We thus speculated that DCP2 might catalyze the decapping of LINE-1 RNA and thus trigger LINE-1 RNA degradation (Fig 2). To test this, we first measured the decay kinetics of LINE-1 RNA in DCP2-expressing cells as previously reported (Li *et al*, 2013) and found that DCP2 expression significantly reduced the half-life of LINE-1 RNA (Fig 3A), suggesting that DCP2 reduces the stability of LINE-1 RNA. Furthermore, we found that the DCP2 mutant E147/148Q, which contains two conserved glutamic acid residues (E147 and E148) within the catalytic site substituted for glutamine and has lost the decapping function (Wang *et al*, 2002), exhibited no effect on the stability of LINE-1 RNA (Fig 3A), supporting that DCP2 induces decapping of LINE-1 RNA and causes LINE-1 RNA degradation.

To further investigate this mechanism, we performed RT-qPCR to quantify the amount of 5' capped LINE-1 mRNA that can be immunoprecipitated with m7G-cap-specific antibody. To prevent rapid degradation of noncapped RNA in cells (Schoenberg, 2011), we knocked down endogenous *XRN1* with siRNA, so that input RNA levels were similar in the cells with or without DCP2 expression. The data showed that, with the increase in DCP2 expression, the level of capped LINE-1 RNA gradually decreased (Fig 3B). As a control, the inactive DCP2 mutant (E147/148Q) exhibited no effect on the level of capped LINE-1 RNA (Fig 3C), indicating that the reduction in capped LINE-1 RNA by DCP2 depends on its decapping activity. In turn, knocking down endogenous DCP2 increased the level of capped LINE-1 RNA and virtually eliminated the inhibitory effect of MOV10 on the capped LINE-1 RNA (Fig 3D). Collectively, these results suggest that DCP2 can cause decapping of LINE-1 RNA.

In further support of the cooperative action of MOV10 and DCP2 in degrading LINE-1 RNA (Fig 2), overexpression of MOV10 resulted in a dose-dependent decrease in the level of capped LINE-1 RNA (Fig 3E), whereas knockdown of MOV10 increased the level of capped LINE-1 RNA compared to that in control cells (Fig 3F). Importantly, we found that in the MOV10-KD cells, increasing the expression of DCP2 did not affect the level of capped LINE-1 RNA (Fig 3G). These results suggest that MOV10 links DCP2 to LINE-1 RNA, causing LINE-1 RNA decapping and degradation. Of note, two MOV10 mutants (MOV10KR and MOV10EQ), which have the amino acids Lys-530 and Glu-647 mutated to Arg and Gln, previously shown deficient in inhibiting LINE-1 (Li *et al*, 2013), did not enhance DCP2-mediated decapping of LINE-1 RNA (Fig 3H), further supporting the important role of MOV10 in DCP2-mediated

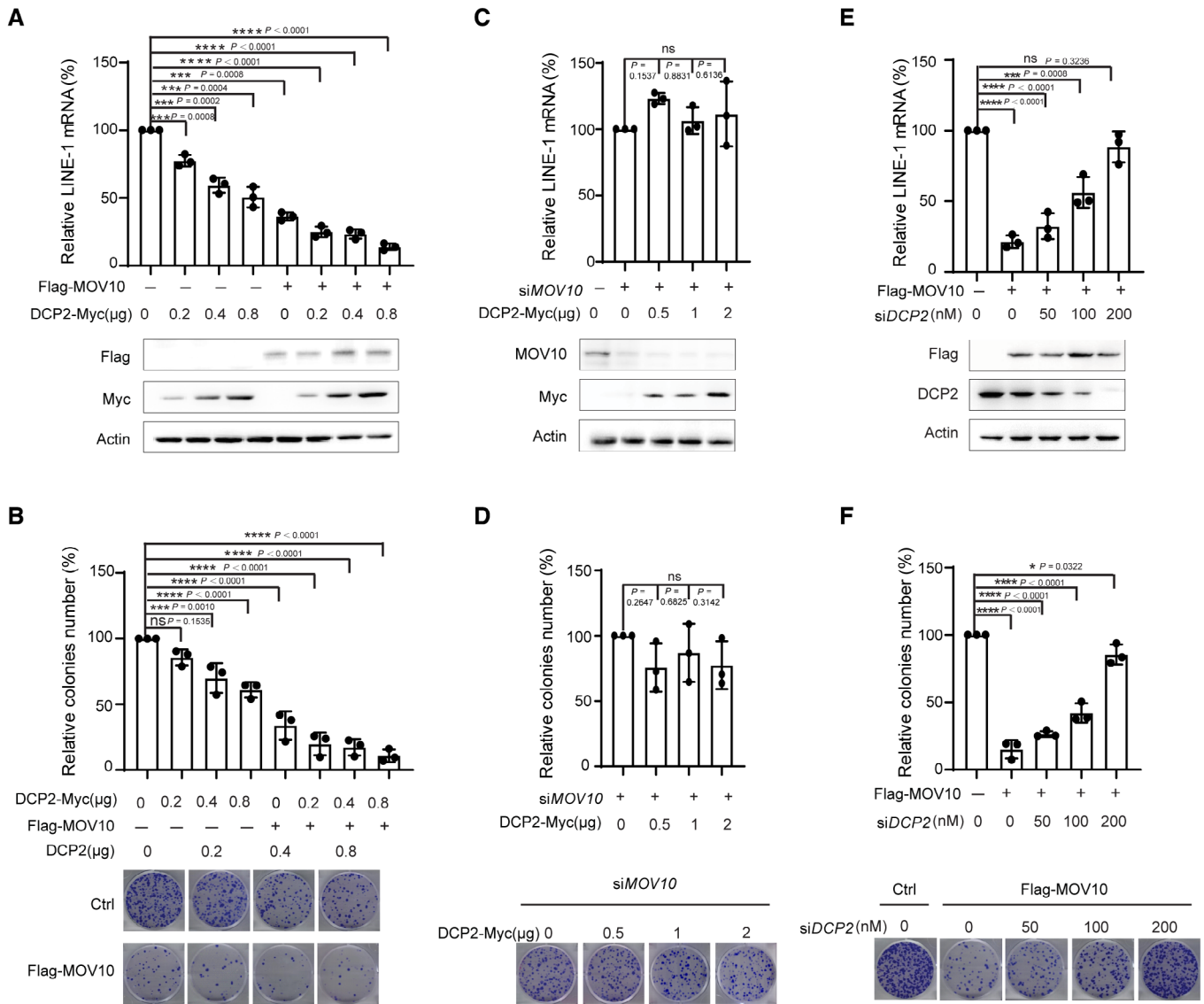


Figure 2. DCP2 cooperates with MOV10 in the degradation of LINE-1 RNA and the inhibition of LINE-1 retrotransposition.

A, B Overexpression of DCP2 diminished LINE-1 RNA level and inhibited LINE-1 retrotransposition in HeLa cells. HeLa cells were cotransfected with CMV-L1-neo^{RT} and increasing amounts of plasmids expressing DCP2 and with or without MOV10 DNA. Cells were subjected to RNA isolation, Western blots, and LINE-1 retrotransposition assay. LINE-1 RNA was quantified by RT-qPCR and normalized to GAPDH expression. Western blots were probed with antibodies for the detection of MOV10 (anti-Flag), DCP2 (anti-Myc), and actin expression. In LINE-1 retrotransposition assay, the colony numbers were visualized with crystal violet staining, the results represent LINE-1 mobilization activity. The data from three independent experiments were summarized in the bar graph. The number of cell colonies in the absence of MOV10 was arbitrarily set as 100. $n = 3$ biological replicates.

C, D MOV10 is required for the LINE-1 inhibitory activity of DCP2. HeLa cells were transfected with *MOV10* siRNAs or nontargeting control siRNA, and then were cotransfected with CMV-L1-neo^{RT} and increasing amount of plasmids expressing DCP2. 48 h later, the cells were subjected to RNA isolation, Western blots, and LINE-1 retrotransposition assay. LINE-1 RNA was quantified by RT-qPCR and normalized to GAPDH expression. The number of cell colonies in the absence of MOV10 was arbitrarily set as 100. $n = 3$ biological replicates.

E, F DCP2 is required for the LINE-1 inhibitory activity of MOV10. HeLa cells were transfected with increasing amounts of *DCP2* siRNAs or nontargeting control siRNA, and then cotransfected with CMV-L1-neo^{RT} and MOV10 DNA. The cells were subjected RNA isolation, Western blots, and LINE-1 retrotransposition assay. LINE-1 RNA was quantified by RT-qPCR and normalized to GAPDH expression. The number of cell colonies in the absence of MOV10 was arbitrarily set as 100. $n = 3$ biological replicates.

Data information: Error bars indicate SD, P -value was determined using ordinary one-way ANOVA test. * $P < 0.05$; ** $P < 0.01$; *** $P < 0.001$; **** $P < 0.0001$.

Source data are available online for this figure.

decapping. In addition, we did not observe any effect on the level of capped GAPDH mRNA with overexpression or knockdown of either MOV10 or DCP2 (Fig EV3A–G). This suggests that the MOV10-Dcp2

complex exerts a decapping activity on a possible subset of mRNAs including LINE-1 mRNA rather than general effect on all cellular mRNA.

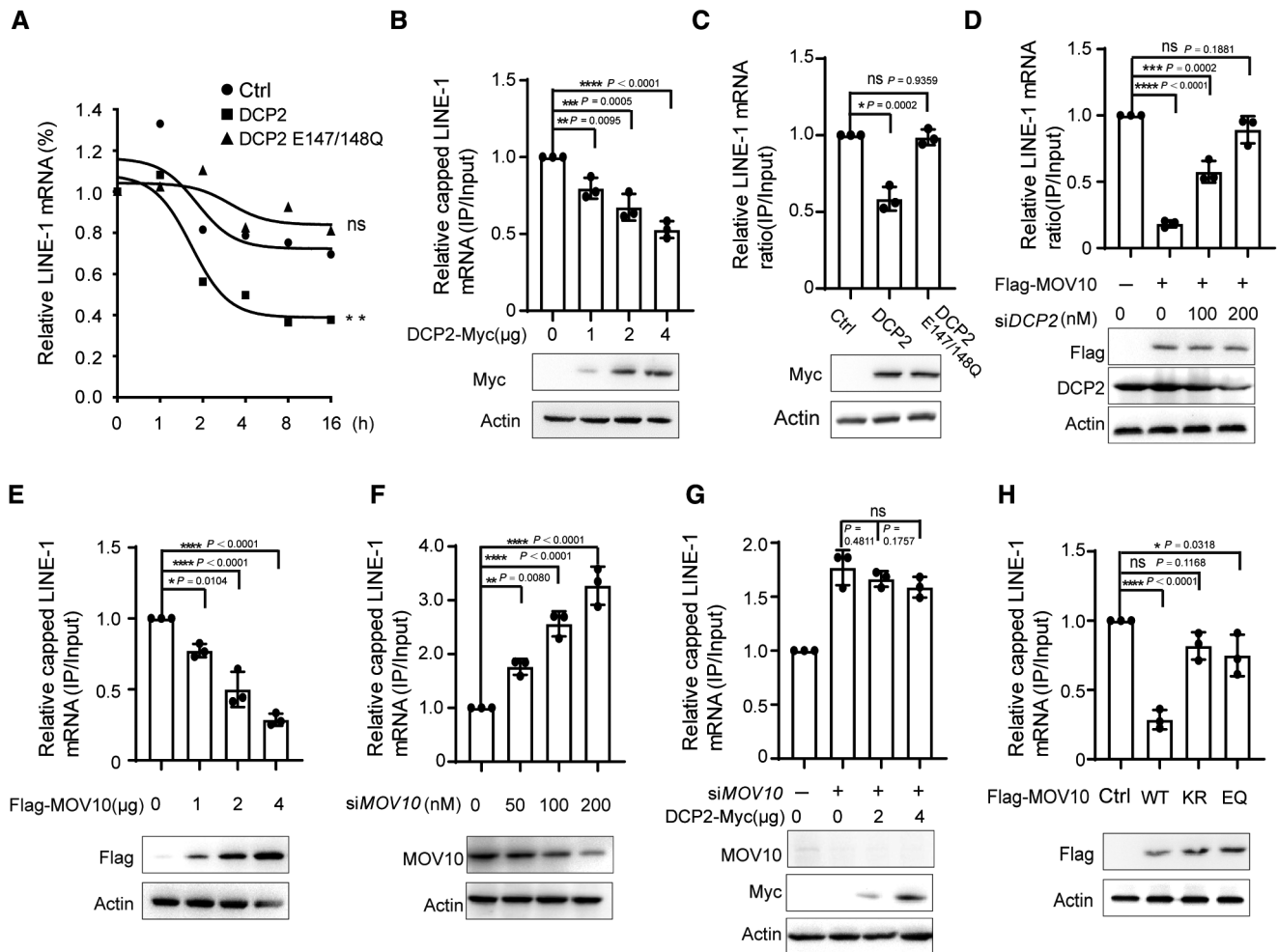


Figure 3. DCP2 decaps LINE-1 RNA in the presence of MOV10.

- A The decay kinetics of LINE-1 RNA in the presence of DCP2 or its mutant DCP2 (E147/148Q). HEK293T cells were cotransfected with CMV-L1-neo^{RT} and DCP2-Myc, DCP2 (E147/148Q)-Myc or empty vector control pCDNA4. Cells were collected at 0, 1, 2, 4, 8 and 16 h post-transfection for LINE-1 mRNA level detection using RT-qPCR.
- B The level of capped LINE-1 RNA in the presence of DCP2. The HEK293T cells were treated with *XRN1* specific siRNAs, and then transfected with CMV-L1-neo^{RT} and different amounts of DCP2-Myc or DCP2 (E147/148Q)-Myc. The cell lysate was collected for RNA immunoprecipitation using m7G-cap-specific antibody. The input and immunoprecipitated RNA were quantified for LINE-1 RNA level by RT-qPCR, and the ratio of immunoprecipitated LINE-1 RNA to total LINE-1 RNA represent the capped LINE-1 RNA Level ($n = 3$ biological replicates).
- C The level of capped LINE-1 RNA in the presence of DCP2 (E147/148Q) comparing to WT DCP2 ($n = 3$ biological replicates).
- D Knocking down endogenous *DCP2* by specific siRNA increased the level of capped LINE-1 RNA ($n = 3$ biological replicates).
- E Overexpression of MOV10 resulted in a dose-dependent decrease of capped LINE-1 RNA ($n = 3$ biological replicates).
- F Knocking down of MOV10 increased the level of capped LINE-1 RNA ($n = 3$ biological replicates).
- G In the MOV10-knockdown cells, the increased expression of DCP2-Myc did not affect the m7G-cap cap level of LINE-1 RNA ($n = 3$ biological replicates).
- H MOV10 mutants (MOV10KR and MOV10EQ) did not stimulate DCP2-mediated decapping of LINE-1 RNA ($n = 3$ biological replicates).

Data information: Error bars indicate SD, P -value was determined using ordinary one-way ANOVA test. * $P < 0.05$; ** $P < 0.01$; *** $P < 0.001$; **** $P < 0.0001$. Source data are available online for this figure.

Next, we investigated whether DCP2 and MOV10 catalyze the decapping of endogenous LINE-1 RNA by RNAiP as previously described. T47D cells, a breast cancer cell line that has a relatively high level of cytoplasmic LINE-1 expression (Chen *et al.*, 2020), were transfected with plasmids expressing Flag-MOV10, DCP2-Myc, or the two both, followed by immunoprecipitated with m7G-cap-specific antibody. The data show that with MOV10 and DCP2 expression, the level of capped LINE-1 RNA decreased to 50%, but not the

GAPDH mRNA, suggesting that MOV10 and DCP2 work together to decap endogenous LINE-1 mRNA (Fig EV3H–J).

MOV10 initiates the formation of a DCP2/MOV10/LINE-1 RNP complex

MOV10 has been shown to interact with LINE-1 RNP through binding to ORF1 in an RNA-dependent manner (Goodier *et al.*, 2012).

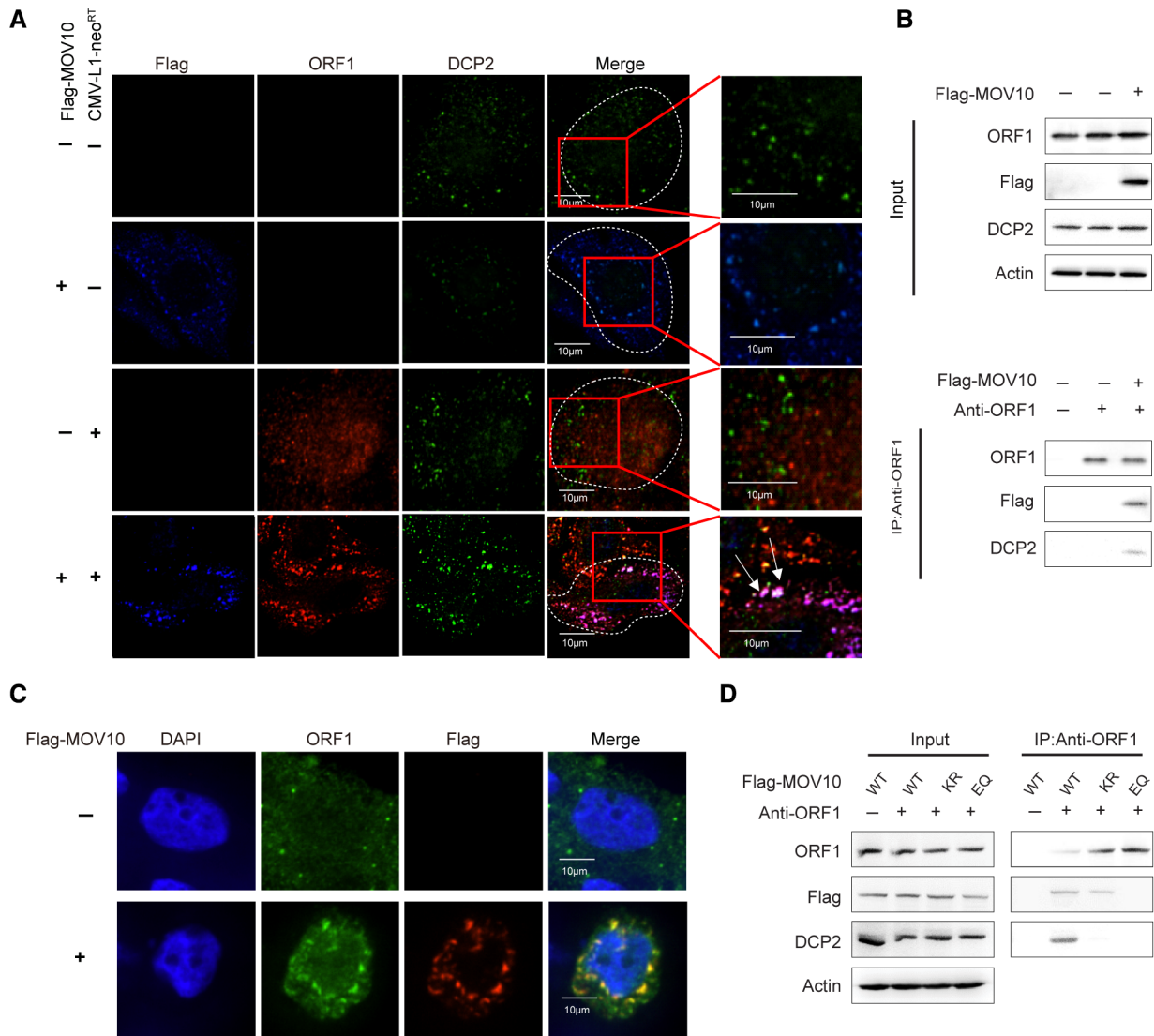


Figure 4. MOV10 promotes the formation of complex of MOV10/LINE-1 RNP/DCP2.

A Subcellular localization of MOV10, LINE-1 ORF1, and DCP2. HeLa cells were transfected with CMV-L1-neo^{RT} and Flag-MOV10 plasmids. Immunofluorescence confocal microscopy was performed to determine the subcellular localization of MOV10 (blue), ORF1 (Red), and DCP2 (Green). Scale bars represent 10 μ m.

B MOV10-mediated the interaction between the LINE-1 RNP, and DCP2. HEK293T cells were cotransfected CMV-L1-neo^{RT} with or without Flag-MOV10, and the cell lysate was subjected to immunoprecipitation with anti-ORF1 antibody (Rabbit). Input and anti-ORF1 IPs were examined in immunoblot using antibodies against ORF1p, Flag, and DCP2.

C MOV10 is capable of inducing the formation of DMLC with endogenous LINE-1 in T47D cells. Confocal microscopy showed subcellular localization of MOV10 (red) and ORF1p (Green). Scale bars represent 10 μ m.

D CMV-L1-neo^{RT} was cotransfected with Flag-MOV10 or its mutant Flag-MOV10 (KR) or Flag-MOV10 (EQ) in HEK293T cells. Immunoprecipitation was performed with anti-ORF1 antibody. Input and anti-ORF1 IPs were subjected to immunoblot analysis using antibodies against ORF1p, Flag, and DCP2.

Source data are available online for this figure.

Considering the interaction of MOV10 with DCP2 (Fig 1), we hypothesized that MOV10 bridges the formation of a DCP2/MOV10/LINE-1 RNP complex (hereafter named DMLC), allowing DCP2 to access LINE-1 RNA, followed by decapping and degradation reactions. Indeed, we observed the colocalization of LINE-1 ORF1p, DCP2, and MOV10 in larger cytoplasmic granules, with very high Pearson's colocalization coefficient values (Fig 4A). In contrast, in the absence of MOV10 overexpression, the majority of LINE-1

ORF1p and DCP2 were enriched in cytoplasmic foci, but not colocalized (Fig 4A), suggesting that MOV10 is required to form DMLC. This is further supported by the results of a Pearson's colocalization analysis showing an approximate 2.5-fold increase in the percentage of LINE-1 ORF1p (red) colocalization with DCP2 (green) in the presence of MOV10 compared with the control group without MOV10 overexpression (Fig EV4A). The key role of MOV10 in DMLC formation was further confirmed by examining the association between

Figure 5. MOV10 induces the formation of DMLC-containing granules through liquid–liquid phase separation.

- A The size of DMLC-containing granule and that of LINE-1 containing stress granule (SG) in Fig 4A ($n = 115$ Ctrl, 77 MOV10).
- B HeLa cells transfected with CMV-L1-neo^{RT} and Flag-MOV10 plasmids were treated with 1,6-hexanediol and then performed immunofluorescence to detect the DMLC-containing granule formation, ORF1p (Red) and MOV10 (Green) ($n = 3$ technical replicates). Scale bars represent 20 μm .
- C The effect of 1,6-hexanediol to small cellular foci formed by either ORF1p or MOV10 alone. HeLa cells were transfected with Flag-MOV10 or CMV-L1-neo^{RT} alone, and then examined with immunofluorescence. LINE-1 ORF1 is shown in red, MOV10 in green ($n = 3$ technical replicates). Scale bars represent 20 μm .
- D Upon removal of the LCD region from ORF1p, MOV10 was unable to induce the formation of large granules. HeLa cells were transfected with Flag-MOV10 and CMV-L1-neo^{RT} or its mutant which lost the LCD region from ORF1p and then examined with immunofluorescence to detect the DMLC-containing granule formation. ORF1p is shown in red, MOV10 in green ($n = 3$ technical replicates). Scale bars represent 10 μm .
- E Diagram of LINE-1 ORF1 and ORF1(157–338). ORF1 consists of threefolded domains: a coiled-coil region responsible for trimerization, an RRM, and a CTD, which act in concert to bind to LINE-1 RNA. The intrinsically disordered N-terminal region is denoted as IDR.
- F MOV10 can promote phase separation of the full-length ORF1 protein in 300 mM NaCl but can not promote phase separation of the ORF1(157–338) protein. Scale bars represent 100 μm .
- G The size of droplets of ORF1 samples and ORF1 with MOV10 samples ($n = 119$ ORF1, 92 ORF1 + MOV10).

Data information: Error bars indicate SD, P -value was determined using unpaired t test. **** means $P < 0.0001$.

Source data are available online for this figure.

DCP2 and LINE-1 RNP with or without MOV10 in 293T cells in the co-IP experiment. The results showed that DCP2 was only detected in the immunoprecipitated materials using the LINE-1 ORF1p-specific antibody with MOV10 overexpression, and virtually no DCP2 was found without MOV10 overexpression (Fig 4B). In agreement with the inability of two MOV10 mutants, MOV10KR and MOV10EQ, to interact with DCP2, their expression did not promote the interaction between ORF1p and DCP2 (Fig 4D). This suggests that RNA helicase domain of MOV10 play a role in its interaction with DCP2, consequently, recruit DCP2 to LINE-1 RNA for decapping. In addition to ectopic expression of LINE-1, we also examined whether MOV10 is capable of inducing the formation of DMLC with endogenous LINE-1 in T47D cells. The imaging data showed that only in the cells expressing MOV10, ORF1, and DCP2 colocalized with MOV10 in large cytoplasmic foci (Fig 4C). Collectively, these results demonstrate the important role of MOV10 in the formation of DMLC.

We also investigated whether LINE-1 RNA was also a part of the large cytoplasmic granules using a LINE-1-MS2 DNA construct, in which two copies of the binding sites for MS2 bacteriophage coat protein were inserted just downstream of the LINE-1 ORF2. Upon co-expression of an MS2-GFP fusion protein, the interaction of the MS2-GFP protein with the MS2 sites in the LINE-1 RNA allows the detection of the tagged RNA by microscopy (Fig EV4B; Bertrand et al, 1998). In addition, the results of RNAIP show that ORF1, DCP2, and LINE-1 RNA were all detected in the immunoprecipitated materials using the antibody against MOV10 (Fig EV4C and D). Collectively, these results suggest that LINE-1 mRNA was associated with DCP2/MOV10/LINE-1 complex as RNPs.

Formation of DMLC-containing granules involves liquid–liquid phase separation

Previous studies have shown that both ectopically expressed and endogenous ORF1p accumulate in cytoplasmic foci, costaining with stress granule (SG) markers (Goodier et al, 2007), while the yeast Ty3 retrotransposon has been shown to associate with cytoplasmic P-bodies (PB) (Beliakova-Bethell et al, 2006). However, the DMLC-containing granules did not appear to be typical SGs, since the average size of DMLC-containing granules was much larger than that of the LINE-1 ORF1p-containing SGs (Fig 5A). To characterize the nature of this type of granule, we hypothesized that the DMLC-

containing granules may possess the feature of liquid–liquid phase separation (LLPS), a mechanism that governs the formation of membrane-less compartments in cells. Several lines of evidence have suggested that RNP bodies and other membrane-less organelles are formed via LLPS in a concentration-dependent manner (Brangwynne et al, 2009; Wippich et al, 2013; Molliex et al, 2015; Nott et al, 2015; Weber & Brangwynne, 2015). Indeed, the MOV10-induced large cellular granules almost completely disappeared following the treatment with 1,6-hexanediol (Fig 5B), a compound that is known to perturb weak hydrophobic interactions and disassemble structures that exhibit liquid phase separation properties (Ribbeck & Gorlich, 2002; Patel et al, 2007). In contrast, the smaller cellular foci formed by either ORF1p or MOV10 alone were not affected by 1,6-hexanediol (Fig 5C). These data support the LLPS nature of the DMLC-containing granules.

Recent reports have shown that proteins containing low complexity sequence domains (LCDs) tend to undergo LLPS (Elbaum-Garfinkle et al, 2015; Nott et al, 2015; Alberti et al, 2019). Using the prediction program IUPred2A (<https://iupred2a.elte.hu/>), we found an LCD within LINE-1 ORF1p, which consists of amino acids RELREECRSLRSRC. The removal of the LCD region from ORF1p prevented MOV10 from forming large granules (Fig 5D). Meanwhile, we found that attaching the ORF1p LCD to GFP (Fig EV4E) did not enable the formation of large cellular foci in the presence of MOV10 (Fig EV4F), suggesting that the LCD of ORF1p is essential but not sufficient for LLPS-driven formation of DMLC-containing granules.

Next, we asked whether MOV10 promote ORF1 to form phase-separated droplets *in vitro*. We purified the MOV10, ORF1, and ORF1(157–338) from *Escherichia coli*. ORF1(157–338), a mutant that has the coiled coil domain deleted and lose the ability to form phase separated droplets, was used as a control (Fig 5E) (Newton et al, 2021). The images showed that MOV10 and full-length ORF1 protein together increased the size of the phase separated droplets in comparison with full-length ORF1 only (Fig 5F and G). The results support that MOV10 can promote phase separation of the full-length ORF1 protein.

Given the LLPS property of SG marker protein G3BP and its presence in the ORF1p-containing cytoplasmic foci (Goodier et al, 2007), we examined the possible role of G3BP1 in driving the formation of DMLC-containing granules. We first investigated the localization of G3BP1 with DMLC-containing granules, using the PB marker GW182 as a control. As shown in Fig 6A, G3BP1 markedly

colocalized with DMLC that were costained with ORF1p and MOV10. Although ORF1p or MOV10 alone was also found to colocalize with G3BP1, these cytoplasmic foci tended to be much smaller than DMLC and partially overlapped. Unlike G3BP1, only a portion of GW182 colocalized with DMLC (Fig 6B). Although ORF1p alone

can form cytoplasmic foci containing G3BP1, overexpression of MOV10 increased the amount of ORF1p in G3BP1-immunoprecipitated materials (Fig 6C), which was corroborated by the twofold reduction of ORF1p in G3BP1-immunoprecipitation when MOV10 was knocked down (Fig 6D). Importantly, when

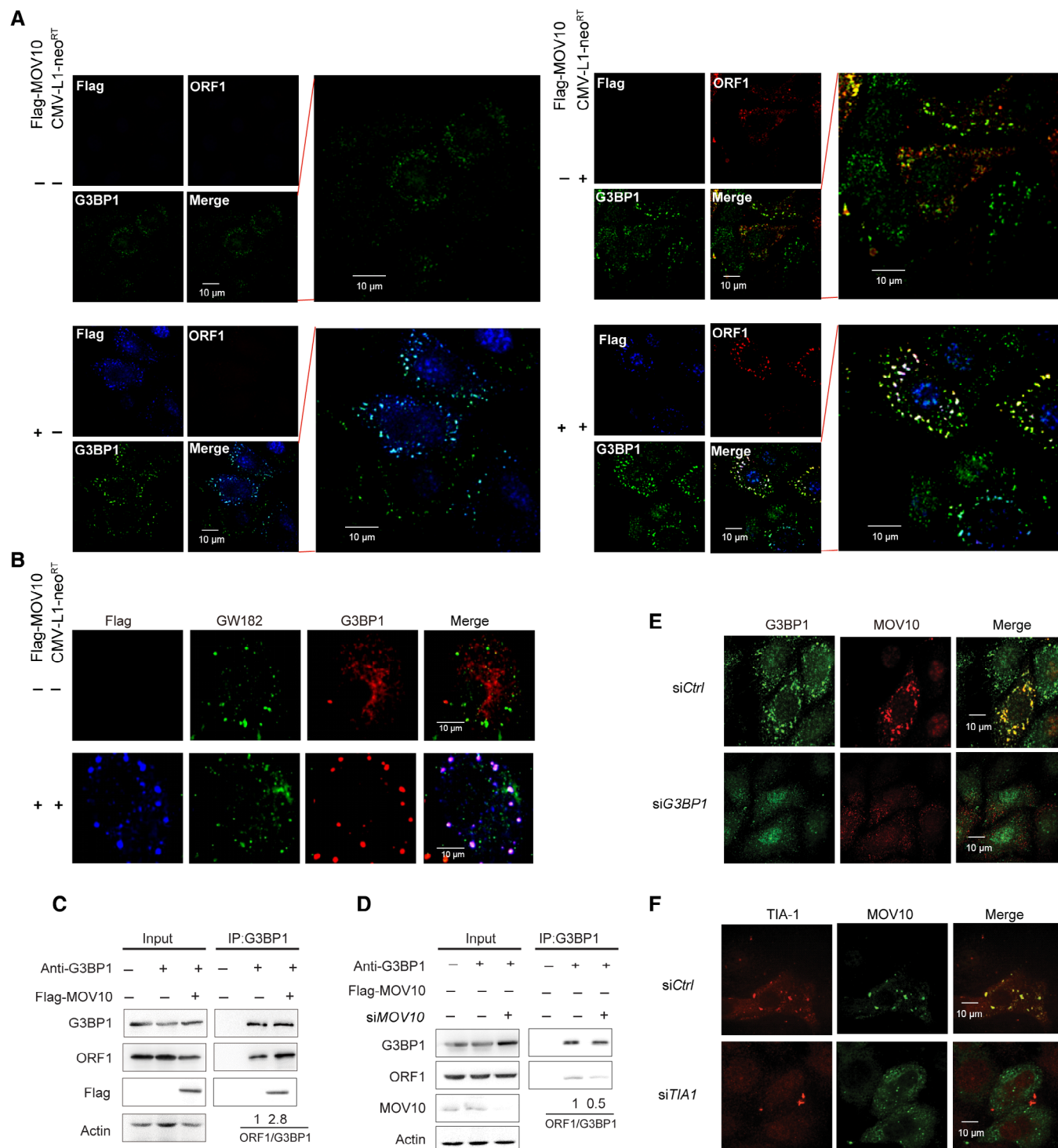


Figure 6.

Figure 6. G3BP1 plays an important role in LLPS-driven formation of DMLC-containing granules.

- A G3BP1 was colocalized with DMLC-containing granule in the presence of MOV10. Confocal images showing cytoplasmic localization of MOV10, LINE-1 ORF1p, and G3BP1 using anti-Flag, anti-ORF1p, and anti-G3BP1 antibodies.
- B Only a portion of GW182 colocalized with DMLC. Confocal images showing cytoplasmic localization of MOV10, GW182, and G3BP1 using anti-Flag, anti-GW182, and anti-G3BP1 antibodies.
- C Interactions among LINE-1 ORF1p, MOV10, and G3BP1. HEK293T cells were cotransfected with CMV-L1-neo^{RT} and MOV10 DNA or empty vector. Input and anti-G3BP1 IPs were subjected to immunoblot analysis using antibodies against G3BP1, MOV10, and ORF1p.
- D Interactions among LINE-1 ORF1, G3BP1, and endogenous MOV10. Endogenous MOV10 was knockeddown by using siRNA in HEK293T cells. Input and anti-G3bp1 IPs were subjected to immunoblot analysis using antibodies against G3BP1, MOV10, and ORF1p.
- E Knocking down the endogenous G3BP1 prevents the formation of DMLC-containing granule.
- F Confocal images showing that silencing TIA1 by siRNA diminished DMLC-containing granule using anti-MOV10 and anti-TIA1 antibodies.

Source data are available online for this figure.

G3BP1 was knocked down with siRNA, DMLC was not observed (Fig 6E). A similar observation was made with another SG marker protein, TIA1, which was also colocalized with DMLC (Fig 6F). Together, these data demonstrate the LLPS nature of DMLC, and the crucial role of the LCD of ORF1p and SG marker proteins G3BP1 and TIA1 in assisting the formation of DMLC.

DMLC granules play a key role in MOV10-mediated restriction of LINE-1

The knocking down of G3BP1 or TIA1 disperses DMLC granules, and this provides an opportunity to test their role in the formation of this LLPS structure in MOV10-mediated restriction of LINE-1 activity. Accordingly, we cotransfected 293T cells with plasmids expressing LINE-1 and MOV10, and increasing amounts of G3BP1 siRNA, and examined the level of capped LINE-1 RNA level, as well as LINE-1 retrotransposition. The results showed that with the gradual reduction in endogenous G3BP1, the inhibitory effect of MOV10 on LINE-1 RNA level (Fig 7A) and LINE-1 retrotransposition (Fig 7B) consistently diminished. When the majority of G3BP1 was depleted by siRNA, MOV10 completely failed to inhibit LINE-1. In a similar vein, silencing TIA1 by siRNA also diminished the inhibitory effect of MOV10 on LINE-1 RNA level (Fig 7C) and LINE-1 retrotransposition (Fig 7D). In contrast, silencing of the P-body protein GW182 by siRNA, which did not colocalize with the DMLC granules (Fig 6B), had no effect on the MOV10 restriction of LINE-1 (Fig EV5A). Moreover, depletion of either G3BP1 or TIA1 restored the level of capped LINE-1 RNA in the presence of

MOV10 (Fig 7E and F), but had no effect on the decapping of GM-CSF mRNA (Fig 7G and H), which was reported previously to be decapped by DCP2 (Lykke-Andersen & Wagner, 2005). These results support that formation of the MOV10-driven DMLC granules is required for decapping and degrading LINE-1 RNA by DCP2, as well as restriction of LINE-1.

Discussion

In this study, we identified DCP2, a main RNA decapping enzyme, as a key cofactor in MOV10-mediated restriction of LINE-1 retrotransposition. MOV10 provides an important defense mechanism controlling the activity of LINE-1, and this function of MOV10 is facilitated by host factors, including UPF1, RNASEH2, and TUT4/7 (Arjan-Odedra et al, 2012; Goodier et al, 2012; Lu et al, 2012; Li et al, 2013; Gregersen et al, 2014; Skariah et al, 2017; Choi et al, 2018; Warkocki et al, 2018). We previously reported that MOV10 inhibits LINE-1 by reducing the level of LINE-1 RNA (Li et al, 2013), yet the underlying molecular mechanism remains undetermined. We now report that MOV10 recruits DCP2 to the LINE-1 RNP, and together form DMLC granules with the feature of LLPS, followed by DCP2 decapping and degradation of LINE-1 RNA through a noncanonical RNA 5' to 3' decay pathway, leading to restriction of LINE-1 retrotransposition (Fig 8).

Our data support the hypothesis that MOV10 binds to LINE-1 RNA and recruits DCP2 to the 5' end of LINE-1 RNA for decapping (Gregersen et al, 2014). It has been reported that MOV10 binds to

Figure 7. DMLC-containing granules play a key role in MOV10-mediated restriction on LINE-1.

- A, B Silencing the endogenous G3BP1 eliminated the inhibition of LINE-1 RNA expression by MOV10. HEK293T cells were treated with different amounts of G3BP1 siRNA or nontargeting control siRNA, and then were cotransfected with CMV-L1-neo^{RT} and MOV10 DNA. The cells were harvested for LINE-1 RNA detection, Western blots, and LINE-1 retrotransposition assay. LINE-1 RNA was quantified by RT-qPCR and normalized to GAPDH expression. The number of cell colonies in the absence of MOV10 was arbitrarily set as 100 ($n = 3$ biological replicates).
- C, D Silencing the endogenous TIA1 nullified MOV10 inhibition of LINE-1 RNA expression and LINE-1 retrotransposition. LINE-1 RNA was quantified by RT-qPCR and normalized to GAPDH expression. The number of cell colonies in the absence of MOV10 was arbitrarily set as 100 ($n = 3$ biological replicates).
- E, G Silencing the endogenous G3BP1 restored the level of capped LINE-1 RNA in the presence of MOV10, but had no effect on the decapping of GM-CSF mRNA by DCP2 ($n = 3$ biological replicates).
- F, H Knocking down the endogenous TIA1 rescued the level of capped LINE-1 RNA in the presence of MOV10, but did not rescue the decapping of GM-CSF mRNA by DCP2 ($n = 3$ biological replicates).

Data information: Error bars indicate SD, P -value was determined using ordinary one-way ANOVA test. * $P < 0.05$; ** $P < 0.01$; *** $P < 0.001$; **** $P < 0.0001$.

Source data are available online for this figure.

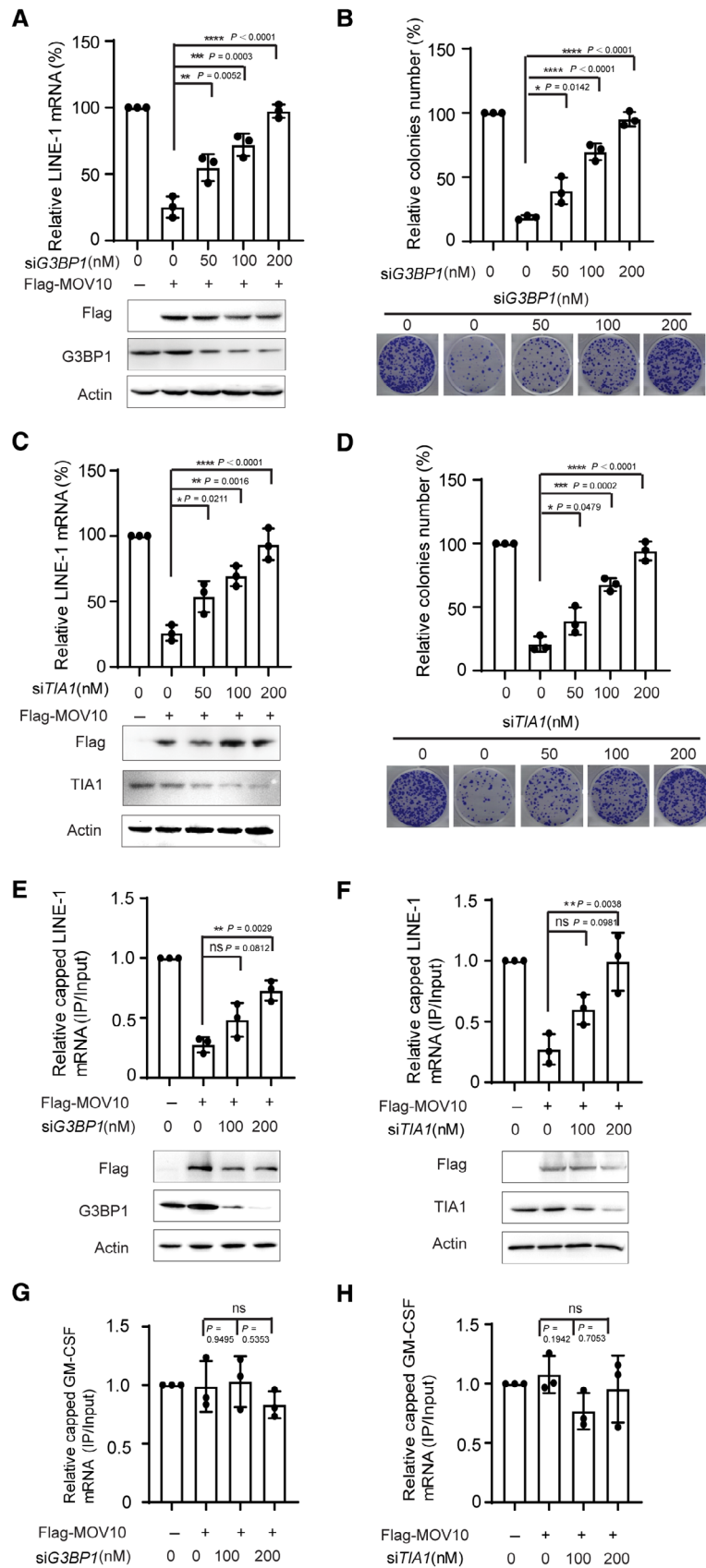


Figure 7.

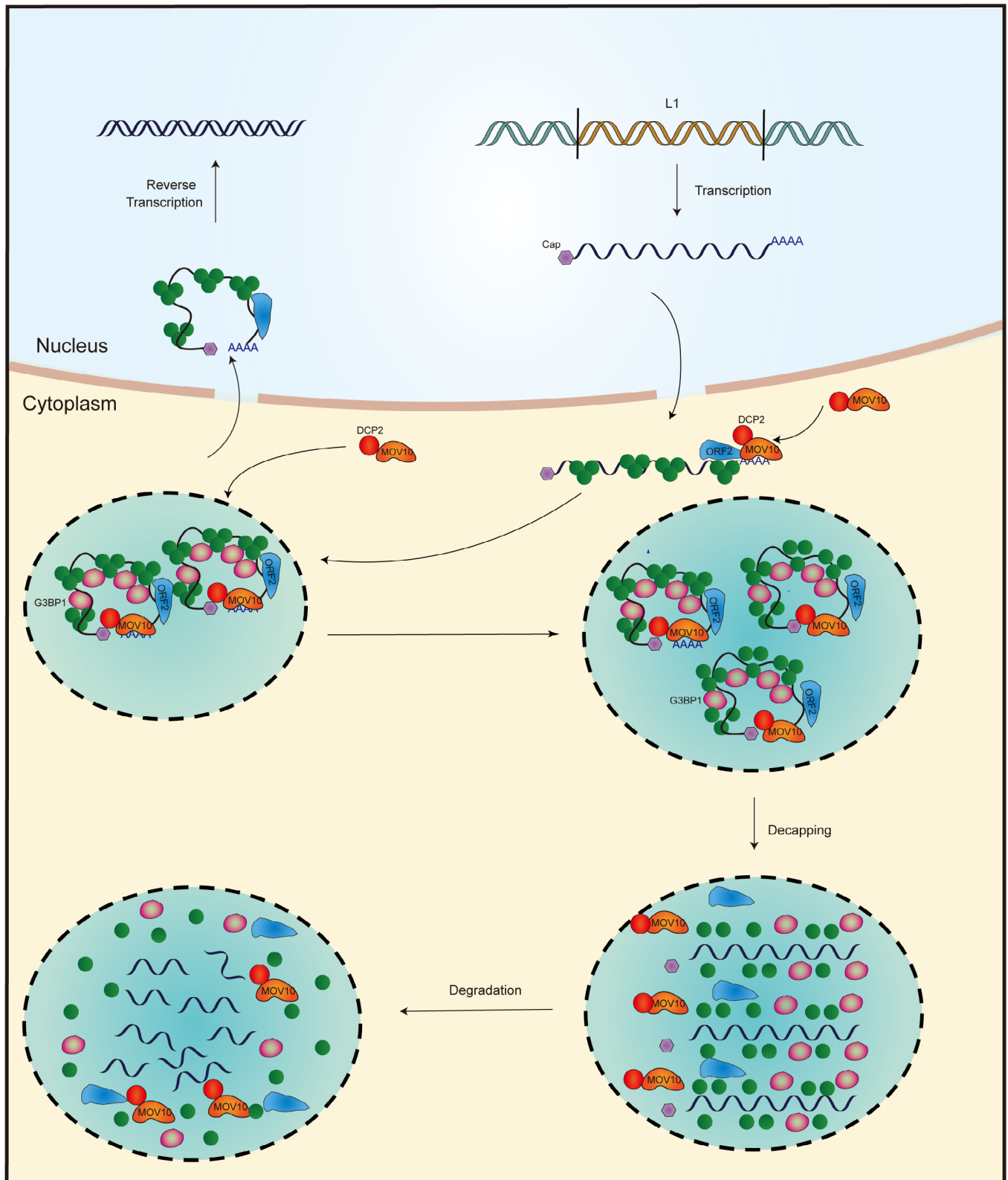


Figure 8. Model illustrating the restriction of LINE-1 retrotransposition by MOV10. MOV10 recruits DCP2 to LINE-1, resulting in the formation of DMLC-containing granules driven by LLPS, which leads to decapping LINE-1 RNA by DCP2 in a noncanonical mechanism, culminating in the degradation of LINE-1 RNA and inhibition of LINE-1 retrotransposition.

the 3' UTR of mRNA, upstream of regions predicted to form local secondary structures, and that knockdown of MOV10 increases the half-life of these MOV10-bound RNA transcripts (Gregersen *et al*, 2014). One possibility is that MOV10 employs a mechanism similar to that of the Pat1-Lsm1-7 or the CCR4-NOT complexes, which are also associated with the 3' end of mRNA, recruit DCP2, and cause mRNA decapping. In addition, as an RNA helicase, MOV10 can open up RNA secondary and tertiary structures and displace the bound ORF1p (Gregersen *et al*, 2014) (Callahan *et al*, 2012), thus negating the protection by ORF1p and exposing LINE-1 RNA to decapping and degradation complexes.

Upon removal of the 5' cap by DCP2, the XRN1 exoribonuclease degrades mRNA in the 5' to 3' direction. We observed the enrichment of XRN1 in the DMLC granules (Fig EV5B). In addition, knockdown of *XRN1* increased the level of LINE-1 RNA (Fig 4A). These data indicate that XRN1 is drawn to the decapped LINE-1 RNA in DMLC and completes the degradation process.

A recent work revealed that ORF1p is inclined to interact with mRNAs in the P-body (Briggs *et al*, 2021). Together with our finding that a P-body protein DCP2 is present in DMLC-granules, these data imply that DMLC-granules may represent P-body. However, our results showed no other canonical P-body markers in the DMLC-granules (Fig 1F). Deletion of GW182 (scaffold protein of P-bodies) results in disassembly of P-bodies but not the DMLC-granules, and had no effect on the MOV10 restriction of LINE-1 (Fig EV5A). These observations together suggest that multiple forms of LINE-1 RNP containing granules with different functions are present in cells (Taylor & Altukhov, 2018), and DMLC-granules likely represent a new form of cytoplasmic body to control LINE-1 replication.

It is worth to note that beside DMLC granule, several forms of MOV10/LINE-1 containing complex or granules have been reported. According to the observation of Taylor *et al* (Taylor *et al*, 2013; Taylor & Altukhov, 2018; Briggs *et al*, 2021), LINE-1 RNPs interact with diverse host proteins. In some RNase-sensitive RNPs, MOV10 and UPF1 are cocaptured proteins within the mixture of the protein belong to IGF2BP1 granules. IGF2BP1 granules may have the function to sequester and stabilize LINE-1 RNPs in the cytoplasm, a process might favor LINE-1 proliferation over degradation. However, G3BP1, the canonical stress granule marker, is not included in these cocaptured proteins. LINE-1 RNPs have been shown to accumulate in G3BP1 or TIA1-marked cytoplasmic stress granules (Goodier *et al*, 2007; Doucet *et al*, 2010). In this study, we also observed DMLC colocalize and interact with G3BP1 to form DMLC containing granules, which play a key role in MOV10-mediated restriction of LINE-1, suggesting that MOV10 may play different roles in distinct complexes.

We observed that the DMLC granules have LLPS properties, since they were dispersed by the treatment of 1,6-hexanediol, which has been commonly used to dissolve LLPS assemblies. Indeed, recent studies have confirmed that LINE-1 ORF1p is able to form a liquid-like condensed phase *in vitro* and *in vivo*, and ORF1p condensation is necessary for LINE-1 retrotransposition (Newton *et al*, 2021; preprint: Sil *et al*, 2022). We found that the presence of MOV10 resulted in larger droplets than that of ORF1p alone, suggesting that MOV10 can promote phase

separation of the full-length ORF1 protein. Liquid-liquid phase separation can concentrate macromolecules above the saturation concentration (Alberti *et al*, 2019), thus providing a mechanism for increasing the local concentration of DCP2 and other cofactors, and accelerating RNA decapping and degradation. Liquid-liquid phase separation has been shown to facilitate the function of several cellular complexes and structures. For example, the deadenylation activity of the miRISC complex is greatly enhanced when it is phase-separated (Sheu-Gruttaduria & MacRae, 2018). Similarly, the LLPS properties of the centrosome concentrate tubulin to promote microtubule nucleation and growth (Woodruff *et al*, 2017). Stress granules also have LLPS properties, and the marker proteins G3BP1 and TIA1 play a crucial role in the formation of DMLC granules via LLPS. Several lines of evidence support the central role of G3BP in LLPS during SG formation (Hu *et al*, 2015a). TIA1 is an RNA-binding protein containing a prison-like LCD and assembles into membrane-less organelles, including SGs (Taylor *et al*, 2016). DCP2/MOV10/LINE-1 complex granules are clearly distinct from stress granules, not only in their size but also in their composition, which awaits further investigation such as proteomic and transcriptomic characterization. In addition to G3BP1 and TIA1, the formation of DMLC is also dependent on MOV10, ORF1p, and probably other factors. Together, these factors may establish more multivalent interactions between themselves and with LINE-1 RNA, thus accelerating the LLPS process, and/or concentrating a higher amount of materials to facilitate the reactions.

The formation of large DMLC granules is driven by MOV10. An early study showed that RNA concentration, when above a certain threshold, triggers a conformational switch and allows greater G3BP1-RNA interaction, thus propelling SG formation (Hu *et al*, 2015a). And interestingly, we found that LINE-1 content in G3BP1-immunoprecipitated materials directly correlated with MOV10 level (Fig 6D and E), suggesting that MOV10 can concentrate LINE-1 RNA, thus initiating LLPS for the formation of DMLC granules. In addition, MOV10 functions as an RNA clearance factor to displace proteins (Warkocki *et al*, 2018), which may cause exposure of the masked LCD in ORF1p and free RNA from the LINE-1 RNP complex, both of which may favor LLPS.

In addition to DCP2, MOV10 also gains TUT4/7 enzymes access to LINE-1 3' ends by displacing LINE-1 proteins from LINE-1 3' ends, which catalyzes the uridylation of LINE-1 mRNA, inducing LINE-1 RNA degradation (Warkocki *et al*, 2018). Moreover, UPF1, a key factor in nonsense-mediated decay (NMD), was reported to be associated with LINE-1 RNPs (Taylor *et al*, 2013) together with MOV10 (Gregersen *et al*, 2014), suggesting that MOV10 and UPF1 may act together to repress the expression of LINE-1 RNA. Therefore, it appears that MOV10 restricts LINE-1 via multiple mechanisms by recruiting different effector proteins to achieve maximal control of LINE-1 activity.

In summary, our data demonstrate that MOV10 recruits DCP2 to LINE-1 RNA, forming LLPS-driven DMLC granules, which facilitates the decapping of LINE-1 RNA by DCP2 and subsequent degradation of LINE-1 RNA. This work sheds light on a new mechanism controlling LINE-1 mobilization by the host and further highlights the important role of LLPS in cellular RNA metabolism.

Materials and Methods

Reagents and Tools table

Reagent or resource	Source	Identifier
Antibodies		
Monoclonal anti-Flag M2 antibody	Sigma-Aldrich	F3165
Rabbit monoclonal [EPR20018-251] to DDDDK tag	Abcam	ab205606
Goat polyclonal to DDDDK tag (Binds to FLAG® tag sequence)	Abcam	ab1257
Monoclonal Anti-c-Myc antibody produced in mouse	Sigma-Aldrich	M4439
Anti-C-Myc antibody produced in rabbit	Sigma-Aldrich	C3956
Rb pAb to MOV10	Abcam	ab80613
Anti-DCP2/TDT	Abcam	ab28658
G3BP1(H-10) Mouse monoclonal IgG	Santa cruz	sc-365338
Rb pAb to TIA1	Abcam	ab40693
Goat polyclonal to CCR4	Abcam	ab1669
Anti-XRN1 antibody produced in rabbit	Sigma-Aldrich	SAB4200028
Rb pAb to DCP1 α	Abcam	ab47811
Ms pAb to LSM1	Abcam	ab167194
Rb pAb to EDC3	Abcam	ab168815
Rabbit monoclonal [EPR12146] to DDX6	Abcam	ab174277
Mouse monoclonal [mAbcam 8226] to beta Actin	Abcam	Ab8226
Ms mAb to GW182	Abcam	ab70522
Anti-m3G, m7G-cap, clone H-20 (mouse monoclonal)	Merck Millipore	cat#2912041
Chemicals, peptides, and recombinant proteins		
1,6-hexanediol	Sigma-Aldrich	240117
RNase A	ThermoFisher	EN0531
Lipofectamine 2000	Thermo Fisher Scientific	11668019
Lipofectamine RNAiMAX	Thermo Fisher Scientific	13778150
Transeasy transfection reagent	Innovation	BY816-002
Critical commercial assays		
Takara MutanBEST kit	Takara	R401
Actinomycin D	J&K Scientific	338112
Deposited data		
Immunoprecipitation-coupled mass spectrometry analysis	This paper	N/A
Experimental models: cell lines		
HEK293T	ATCC	CRL-11268
HeLa	ATCC	CCL-2
T47D	ATCC	HTB-133
Oligonucleotides		
siRNA targeting sequence: <i>TIA1</i> : ATGCCCGAGTGGTAAAAGA	Ribobio Co., Ltd	stB0001646A
siRNA targeting sequence: <i>XRN1</i> : GGTGAAGTTCGTCTAGAGA	Ribobio Co., Ltd	stB0001677B
siRNA targeting sequence: <i>DCP2</i> : GGTTGGCACCTAACAAAT	Ribobio Co., Ltd	siG13820112747
siRNA targeting sequence: <i>MOV10</i> : AGACTCGGTCAGGTTCTT	Ribobio Co., Ltd	stB0001633A
siRNA targeting sequence: <i>G3BP1</i> : ACCACCTCATGTTGTTAAA	Ribobio Co., Ltd	stB0001654B

Reagents and Tools table (continued)

Reagent or resource	Source	Identifier
siRNA targeting sequence:GW182 GGAGAGCGATGGTAGTACA	Ribobio Co., Ltd	siBDM1999A
Primer:LCD-GFP Forward: GCGGGATCCATGCGAGAAGCTACGTGAAGAATGCAGAAGCC TCAGGAGCCGATGCGTGAGCAAGGGCGAGGA	This paper	N/A
Primer:hLCD-GFP Forward: GCGGGATCCATGCGAGAAGCTACGTGAAGAATGCGTGAGCAAGGGCGAG	This paper	N/A
Primer:eLCD-GFP Forward: GCGGGATCCATGCCAAGGCTCGAGAAGCTACGTGAAGAATGCAGAAGCCCT CAGGAGCCGATGCGATCAACTGGAGTGAGCAAGGGCGAGGA	This paper	N/A
Primer: LCD-GFP Reverse: AAATATGCGGCCGCTTACTTGTACAGCTCGTCCATGCCGA	This paper	N/A
Primer:ΔLCD-ORF1 fragment 1 Forward GCGGGATCCATGGAGCAGAACTCATCTCTGAAGAGGATCTGATGGGG AAAAACAGAACAGAAAA	This paper	N/A
Primer:ΔLCD-ORF1 fragment 1 Reverse: AGCCTTGGTTTTTCAGTCCATCAGCT	This paper	N/A
Primer:ΔLCD-ORF1 fragment 2 Forward: AAACCAAGGCTGATCAACTGGAAGA	This paper	N/A
Primer:ΔLCD-ORF1 fragment 2 Reverse: AAATATGCGGCCGCTTACATTTTGGCATGATT	This paper	N/A
Primer: Myc-DCP2 E147/148Q Forward: GCTAGAGAGGCTTTTCAACAACTGGTTTTGATA	This paper	N/A
Primer: Myc-DCP2 E147/148Q Reverse: TATCAAACCAGTTTGTGAAAGACCTCTCTAGC	This paper	N/A
Primer: 5'UTR-L1-neo ^{RT} Forward: CCTGCAGGGGAGGAGCAAGATGGCCGAAT	This paper	N/A
Primer: 5'UTR-L1-neo ^{RT} Reverse: GTCGACTCTAGAGGATCCGAAAAAACCCTCCACACCT	This paper	N/A
Primer: L1(D702Y) Forward: TGTCCTGTTTGCAUACGACATGATTGTAT	This paper	N/A
Primer: L1(D702Y) Reverse: ATACAATCATGTCGTATGCAACAGGGACA	This paper	N/A
Primer: pET21a-ORF1 Forward: GGGAAAAACAGAACAGAAAACTG GAAACTCTAAAACGC	This paper	N/A
Primer: pET21a-ORF1 Reverse: AAATAPTGGCGCCGATAGTCCCATATTTCTTGAGGCTTT	This paper	N/A
Primer: pET21a-ORF1(157–338) Forward: CGCGGATCCAATCTACGTCTGATTGGTGACTCTGAAA	This paper	N/A
Primer for RT-PCR:LINE-1 Forward CTGAAGCGGAAGGG ACTG	This paper	N/A
Primer for RT-PCR:LINE-1 Reverse CCTTGAGCCTGGCGAACAG	This paper	N/A
Primer for RT-PCR:LINE-1 5'UTR Forward CTGAAGCGGAAGGG ACTG	This paper	N/A
Primer for RT-PCR:LINE-1 5'UTR Reverse GAGATGAACCCGGTACCTCA	This paper	N/A
Primer for RT-PCR:GAPDH Forward TGACGTGGACATCCGCAAG	This paper	N/A
Primer for RT-PCR:GAPDH Reverse CTGGAAGGTGGACAGCGAGG	This paper	N/A
Primer for RT-PCR:GM-CSF Forward CTTGGCACTGTGGCCT	This paper	N/A
Primer for RT-PCR:GM-CSF Forward GTCTGTAGGCAGGTCGG	This paper	N/A

Reagents and Tools table (continued)

Reagent or resource	Source	Identifier
Recombinant DNA		
Plasmid:Flag-MOV10	This paper	N/A
Flag-MOV10(EQ)	This paper	N/A
Flag-MOV10(KR)	This paper	N/A
CMV-L1-neo ^{RT}	This paper	N/A
Plasmid: ORF1-Myc	This paper	N/A
Plasmid: DCP2-Myc-His	Changsha Youbao Biotechnology Co., Ltd	N/A
Plasmid: DCP2 ^{E147/148Q} -Myc-His	This paper	N/A
Plasmid:ΔLCD ORF1-Myc	This paper	N/A
Plasmid: ORF1 LCD-GFP	This paper	N/A
Plasmid: ORF1 hLCD-GFP	This paper	N/A
Plasmid: ORF1 iLCD-GFP	This paper	N/A
Plasmid: pET21a-ORF1	This paper	N/A
Plasmid: pET21a-ORF1(157-338)	This paper	N/A
Plasmid: 5'UTR-L1-neo ^{RT}	This paper	N/A
Plasmid: CMV-L1-neo ^{RT} (D702Y)	This paper	N/A
Software and algorithms		
Image J	Image J software	https://imagej.nih.gov/ij/
GraphPad Prism 8	GraphPad software	N/A

Methods and Protocols

Plasmids and antibodies

The pcDNA4.0-based MOV10 DNA clone encodes an N-terminal flag-tagged human MOV10 protein. Two MOV10 mutants, MOV10 (KR) and MOV10 (EQ), which have the amino acids Lys-531 and Glu-647 mutated to Arg and Gln, respectively, were constructed using a site-directed mutagenesis kit (Stratagene). CMV-L1-neo^{RT} carries a complete human LINE-1 DNA copy and a neomycin resistance gene inserted just before the 3' UTR of LINE-1 in the opposite direction to the LINE-1 coding sequence. The neomycin resistance gene is inactivated by the presence of a forward intron, which can be removed during RNA splicing, thus producing a functional neomycin resistance gene after reverse transcription and integration. 5' UTR-L1-neo^{RT} plasmid without which is under regulation of its native promoter in 5' UTR. CMV-L1-neo^{RT} (D702Y), a mutant has the 702 amino acids Asp mutated to Tyr, was cloned using site-directed mutagenesis kit. Myc-His-tagged DCP2 was purchased from Changsha Youbao Biotechnology Co., Ltd. pET21a-ORF1 and pET21a-ORF1(157-338) were constructed using HindIII and BamHI double digested products. MOV10 purified from *E. coli* was purchased from Cusabio Technology Co., Ltd. Lipofectamine 2000 (Invitrogen) was used for transient transfection of plasmids into HEK293T cells. Anti-Flag antibody (mouse) and anti-Flag antibody (rabbit) were purchased from Sigma-Aldrich; anti-β-actin antibody (mouse), anti-DCP2 antibody (rabbit), anti-G3BP1 antibody (mouse), anti-XRN1 (rabbit), anti-CCR4 (rabbit), anti-Pat1b (rabbit), anti-LSM1 (mouse), anti-DCP1α (rabbit), anti-EDC3 (rabbit), anti-RCK (rabbit), and anti-GW182 (rabbit) were purchased from Abcam. Anti-m⁷G cap antibody was purchased from Thermo Fisher. ORF1p antibody (rabbit) was generated as previously described (Li

et al, 2013). Alexa Fluor 647-labeled donkey anti-goat antibody, Alexa Fluor 555-labeled donkey anti-rabbit antibody, Alexa Fluor 488-labeled donkey anti-mouse antibody, Alexa Fluor 555-labeled donkey anti-mouse antibody, and Alexa Fluor 488-labeled donkey anti-rabbit antibody were purchased from Life Technologies.

Cell culture

Human embryonic kidney HEK293T cells and HeLa cells were grown at 37°C in Dulbecco's modified Eagle's medium (DMEM; Gibco) supplemented with 10% fetal bovine serum (Gibco) in a humidified incubator at 5% CO₂. T47D cells were grown in Roswell Park Memorial Institute 1640 (RPMI-1640) medium with 10% fetal bovine serum (Gibco) in a humidified incubator at 5% CO₂.

Immunoprecipitation-coupled mass spectrometry analysis

Immunoprecipitation-coupled mass spectrometry analyses were conducted to identify MOV10-interacting proteins. HEK293T cells were cotransfected with 1 μg CMV-L1-neo^{RT} and 3 μg Flag-MOV10 or pcDNA4To. The cells were collected 48-h post-transfection and then lysed in 350 μl of TNT buffer (20 mM Tris-HCl, pH 7.5, 200 mM NaCl, 1% Triton X-100) on ice for 1 h with gentle rotation. Insoluble material was removed by centrifugation at 12,000 g for 30 min, and the supernatants were incubated with 100 μl of EZview Red ANTI-FLAG M2 Affinity Gel (Sigma) overnight with gentle rotation. The beads were washed five times with 1 ml of lysis buffer and then incubated with 200 μg/ml 3 × FLAG peptide (Sigma) for 2 h. The eluents were collected by centrifugation at 12,000 g for 5 min. The samples were subjected to SDS-PAGE analysis and proteins were visualized using Coomassie Brilliant Blue staining.

Mass spectrometry analyses were performed at Shanghai Wayen Biotechnology Co. Ltd. Briefly, each sample was excised into several

gel fragments, and the fragments were incubated with trypsin buffer at 37°C overnight. The peptides were analyzed using an EASY-nLC 1200 coupled to an Orbitrap Fusion Lumos (Thermo Scientific) and Proteome Discoverer 1.4, Mascot server software (Version 2.3, Matrix Science).

Co-immunoprecipitation (Co-IP) assay

HEK293T cells were cotransfected with CMV-L1-neo^{RT} and Flag-MOV10 DNA or empty vector. The cells were collected 48-h post-transfection and then lysed in 350 μ l of TNT buffer (20 mM Tris-HCl, pH 7.5, 200 mM NaCl, 1% Triton X-100) on ice for 1 h with gentle rotation. The insoluble material was pelleted at 12,000 g for 30 min, and the supernatant was transferred into a new tube. Small aliquots from each sample were saved as “input,” and remaining lysates were incubated with 5 μ l of anti-Flag antibody or anti-ORF1p antibody for 16 h at 4°C, followed by the addition of protein A + G-Sepharose (Amersham Biosciences) for 2 h. The immunoprecipitated complex was then washed three times using TNT buffer and phosphate-buffered saline, followed by Western blot analysis using anti-Flag or anti-ORF1p antibody.

Quantification of LINE-1 RNA by RT-qPCR

HeLa cells transfected with plasmid were collected 48 h later, and total RNA was extracted using the Rapture Total RNA kit (Magen Biotechnologies). cDNA was synthesized using Moloney murine leukemia virus (MMLV) reverse transcriptase (Takara), followed by treatment with DNase (Takara). cDNA was quantified using a qPCR kit (Sso Fast Eva Green Supermix, Takara) using the primers 5'-CTGAAGCGGAAGGGACTG-3' and 5'-CCTTGAGCCTGGCGAACAG-3', which were designed to target to neo gene span the Neo cassette intron of the transfected L1 construct such that only LINE-1 cDNA that has been reverse transcribed from the spliced RNA is amplified to avoid the contamination by CMV-L1-neoRT DNA. A second pair of primers 5'-AATAGGAACAGCTCCGGT-3' and 5'-GAGAT-GAACCCGGTACTCA-3' were designed to target to LINE-1 5'UTR.

Western blotting

Cells were lysed with NP-40 buffer (Beyotime). Equal amounts of cell lysate were separated by SDS-PAGE (10%). Proteins were transferred onto a PVDF membrane, blocked with 5% skimmed milk, and probed with primary antibodies, including anti-Flag antibody (diluted 1:5,000), anti-DCP2 antibody (diluted 1:200), anti-ORF1 antibody (diluted 1:1,000), or anti- β -actin antibody (diluted 1:5,000) at 4°C overnight. After washing four times using PBS plus 0.1% Tween 20 (PBST), the membrane was incubated with a 1:5,000 dilution of HRP-conjugated goat-anti-mouse secondary antibody for 1 h at room temperature. After washing four times using PBST, signals were detected using Western Lighting Chem Illustrine Science Reagent.

Retrotransposition assay

HeLa cells were seeded in six-well plates 1 day prior to transfection. The next day, cells were cotransfected with 1,000 ng CMV-L1-neo^{RT} DNA and DCP2-Myc DNA with or without Flag-MOV10. Forty-eight hours later, cells were detached from the plates using trypsin and split for Western blot, RNA isolation, and the retrotransposition assay. Cells for the retrotransposition assay were seeded into six-well plates at serial dilutions (1×10^5 or 2×10^5 per well), and G418 (0.4 mg/ml) was then added to select for resistant cell colonies. After

10–12 days of selection, when cell colonies were clearly visible, the cells were fixed with methanol for 10 min and stained with 0.5% crystal violet (in 25% methanol) for 10 min. The number of colonies represented the transposition efficiency of LINE-1.

RNAIP (rip)

HEK293T cells were transfected with 1,000 ng CMV-L1-neoRT with 500 ng Flag-MOV10, DCP2-Myc or siRNA targeting MOV10 or DCP2. The cells were collected 48-h post-transfection and then lysed in 350 μ l of TNT buffer (20 mM Tris-HCl, pH 7.5, 200 mM NaCl, 1% Triton X-100) on ice for 1 h with gentle rotation. The insoluble material was pelleted at 12,000 g for 30 min, and the supernatant was transferred into a new tube. Small aliquots from each sample were saved as “input,” and remaining lysates were incubated with 5 μ l of anti-m7G-cap antibody/anti-Flag antibody or anti-IgG antibody for 16 h at 4°C, followed by the addition of protein A + G-Sepharose (Amersham Biosciences) for 2 h. The immunoprecipitated complex was then washed three times using TNT buffer and phosphate-buffered saline, followed by RNA extraction using the Rapture Total RNA kit (Magen Biotechnologies). The input and immunoprecipitated RNAs were quantified for LINE-1 RNA level by RT-qPCR. The level of GAPDH mRNA was used to normalize the input mRNA, and the immunoprecipitated LINE-1 RNA was normalized to input LINE-1 mRNA.

Immunofluorescence microscopy

Cells were incubated in a glass-bottom cell culture dish (Nest) before transfection with the indicated plasmid DNA. Forty-eight hours after transfection, cells were fixed with 4% paraformaldehyde (in $1 \times$ phosphate buffered saline) for 15 min at room temperature followed by a 10-min permeabilization using 0.2% TritonX-100 at room temperature. Cells were then incubated for 1 h with anti-FLAG antibody (diluted 1:5,000), anti-G3BP1 antibody (diluted 1:2,000), anti-DCP2 antibody (diluted 1:200), anti-ORF1 antibody (diluted 1:200), or anti-GW182 antibody (diluted 1:200), followed by Alexa Fluor 647-labeled donkey anti-goat antibody, Alexa Fluor 555-labeled donkey anti-rabbit antibody, and Alexa Fluor 488-labeled donkey anti-mouse antibody (1:1,000 dilution). Confocal images were acquired at room temperature using an Olympus IX81 Microsystem.

siRNA knockdown

For knockdown of *MOV10*, *DCP2*, *G3BP1*, *TIA-1*, *XRN1*, and *GW182*, different concentration of siRNA (50, 100, and 200 nM) were transfected into 4×10^6 HEK293T cells or 2×10^6 HeLa cells by use of Lipofectamine RNAi Max (Invitrogen). siRNAs were purchased from Guangzhou Ribobio Co., Ltd. (Guangzhou, China).

CCK8

A CCK-8 kit (meilunbio, Dalian, China) was used to measure proliferation of HeLa cells. Cells treated with MOV10/DCP2 overexpression or knockdown were cultured in a 96-well plate. The CCK-8 reagent (10 μ l) was added to cell culture solution and incubated for 1 h.

Protein expression and purification

ORF1 and its mutant ORF1(157-338) sequences were amplified by PCR and cloned into pET21a vector using BamHI and NotI double digestion. *Escherichia coli* BL21 (DE3) cells containing pET21a-ORF1

and pET21a-ORF1(157–338) were cultured in lysogeny broth (LB) media containing 100 mg/L ampicillin at 37°C for 4 h to an OD600 between 0.7 and 1, and then final concentration of 0.5 mM isopropyl β-D-1-thiogalactopyranoside (IPTG) were added into LB media for overnight culture at 16°C. All cells were harvested by centrifugation at 10,000 rpm for 15 min and resuspended in buffer A (20 mM Tris–HCl [pH 8.0], 300 mM NaCl, 1 mM DTT). Cells were lysed by sonication and removed debris through centrifugation at 10,000 rpm for 15 min.

The supernatants were primarily loaded on HisTrap column (GE Healthcare) with buffer A and eluted with a gradient buffer B (20 mM Tris–HCl [pH 8.0], 300 mM NaCl, 1 mM DTT, 600 mM imidazole). The eluate was subjected to Superdex 200 10/300 Increase column (GE Healthcare) with buffer A for further protein purification and buffer displacement. The final products were concentrated to more than 5 mg/ml and applied for purity analysis by SDS–PAGE. Total purified proteins were stored at –80°C for further use.

In vitro phase separation assay

Samples of ORF1, ORF1(157–338) with or without MOV10 diluting to 300 mM in a buffer of 20 mM Tris (pH 8.0) and 1 mM DTT with 300 mM NaCl were prepared for differential contrast (DIC) microscopy. 5 ml of the sample was spotted onto a glass coverslip for imaging using an Olympus IX81 Microsystem.

Data analysis

IUPred2A is a combined web interface that allows to identify disordered protein regions using IUPred2 and disordered binding regions using ANCHOR2 (<https://iupred2a.elte.hu/>).

Data availability

The mass spectrometry proteomics data have been deposited to the ProteomeXchange Consortium via the PRIDE (Perez-Riverol et al, 2022) partner repository with the dataset identifier PXD041814.

Expanded View for this article is available [online](#).

Acknowledgments

This work was supported by the CAMS Innovation Fund for Medical Sciences (2021-I2M-1-038) and the National Natural Science Foundation of China (31870164).

Author contributions

Shan Cen: Writing – original draft; project administration; writing – review and editing. **Qian Liu:** Data curation; software; formal analysis; investigation; methodology; writing – review and editing. **Dongrong Yi:** Resources; software; methodology. **Jiwei Ding:** Resources; software. **Yang Mao:** Data curation; software; methodology. **Shujie Wang:** Resources. **Ling Ma:** Resources. **Quanjie Li:** Software. **Jing Wang:** Resources; methodology. **Yongxin Zhang:** Resources; methodology. **Jianyuan Zhao:** Resources. **Saisai Guo:** Resources. **Zhenlong Liu:** Resources. **Fei Guo:** Resources. **Dongbin Zhao:** Resources. **Chen Liang:** Validation. **Xiaoyu Li:** Writing – review and editing. **Xiaozhong Peng:** Resources; project administration.

Disclosure and competing interests statement

The authors declare that they have no conflict of interest.

References

- Alberti S, Gladfelter A, Mittag T (2019) Considerations and challenges in studying liquid–liquid phase separation and biomolecular condensates. *Cell* 176: 419–434
- Arjan-Odedra S, Swanson CM, Sherer NM, Wolinsky SM, Malim MH (2012) Endogenous MOV10 inhibits the retrotransposition of endogenous retroelements but not the replication of exogenous retroviruses. *Retrovirology* 9: 53
- Balinsky CA, Schmeisser H, Wells AI, Ganesan S, Jin T, Singh K, Zoon KC (2017) IRAV (FLJ11286), an interferon-stimulated gene with antiviral activity against dengue virus, interacts with MOV10. *J Virol* 91: 91
- Beck CR, Collier P, Macfarlane C, Malig M, Kidd JM, Eichler EE, Badge RM, Moran JV (2010) LINE-1 retrotransposition activity in human genomes. *Cell* 141: 1159–1170
- Belancio VP, Hedges DJ, Deininger P (2008) Mammalian non-LTR retrotransposons: for better or worse, in sickness and in health. *Genome Res* 18: 343–358
- Beliakova-Bethell N, Beckham C, Giddings TH Jr, Winey M, Parker R, Sandmeyer S (2006) Virus-like particles of the Ty3 retrotransposon assemble in association with P-body components. *RNA* 12: 94–101
- Bertrand E, Chartrand P, Schaefer M, Shenoy SM, Singer RH, Long RM (1998) Localization of ASH1 mRNA particles in living yeast. *Mol Cell* 2: 437–445
- Brangwynne CP, Eckmann CR, Courson DS, Rybarska A, Hoegge C, Gharakhani J, Julicher F, Hyman AA (2009) Germline P granules are liquid droplets that localize by controlled dissolution/condensation. *Science* 324: 1729–1732
- Briggs EM, McKerrow W, Mita P, Boeke JD, Logan SK, Fenyö D (2021) RIP-seq reveals LINE-1 ORF1p association with p-body enriched mRNAs. *Mob DNA* 12: 5
- Brouha B, Schustak J, Badge RM, Lutz-Prigge S, Farley AH, Moran JV, Kazazian HH Jr (2003) Hot L1s account for the bulk of retrotransposition in the human population. *Proc Natl Acad Sci USA* 100: 5280–5285
- Burdick R, Smith JL, Chaipan C, Friew Y, Chen J, Venkatachari NJ, Delviks-Frankenberry KA, Hu WS, Pathak VK (2010) P body-associated protein Mov10 inhibits HIV-1 replication at multiple stages. *J Virol* 84: 10241–10253
- Callahan KE, Hickman AB, Jones CE, Ghirlando R, Furano AV (2012) Polymerization and nucleic acid-binding properties of human L1 ORF1 protein. *Nucleic Acids Res* 40: 813–827
- Chen H, Lilley CE, Yu Q, Lee DV, Chou J, Narvaiza I, Landau NR, Weitzman MD (2006) APOBEC3A is a potent inhibitor of adeno-associated virus and retrotransposons. *Curr Biol* 16: 480–485
- Chen N, Zhou M, Dong X, Qu J, Gong F, Han Y, Qiu Y, Wang J, Liu Y, Wei Y et al (2020) Epidemiological and clinical characteristics of 99 cases of 2019 novel coronavirus pneumonia in Wuhan, China: a descriptive study. *Lancet* 395: 507–513
- Choi J, Hwang SY, Ahn K (2018) Interplay between RNASEH2 and MOV10 controls LINE-1 retrotransposition. *Nucleic Acids Res* 46: 1912–1926
- Cost GJ, Feng Q, Jacquier A, Boeke JD (2002) Human L1 element target-primed reverse transcription in vitro. *EMBO J* 21: 5899–5910
- Denli AM, Narvaiza I, Kerman BE, Pena M, Benner C, Marchetto MC, Diedrich JK, Aslanian A, Ma J, Moresco JJ et al (2015) Primate-specific ORF0 contributes to retrotransposon-mediated diversity. *Cell* 163: 583–593
- Dombroski BA, Feng Q, Mathias SL, Sassaman DM, Scott AF, Kazazian HH Jr, Boeke JD (1994) An in vivo assay for the reverse transcriptase of human retrotransposon L1 in *Saccharomyces cerevisiae*. *Mol Cell Biol* 14: 4485–4492
- Doucet AJ, Hulme AE, Sahinovic E, Kulpa DA, Moldovan JB, Kopera HC, Athanikar JN, Hasnaoui M, Bucheton A, Moran JV et al (2010)

- Characterization of LINE-1 ribonucleoprotein particles. *PLoS Genet* 6: e1001150
- Eibaum-Garfinkle S, Kim Y, Szczepaniak K, Chen CC, Eckmann CR, Myong S, Brangwynne CP (2015) The disordered P granule protein LAF-1 drives phase separation into droplets with tunable viscosity and dynamics. *Proc Natl Acad Sci USA* 112: 7189–7194
- Esnault C, Maestre J, Heidmann T (2000) Human LINE retrotransposons generate processed pseudogenes. *Nat Genet* 24: 363–367
- Feng Q, Moran JV, Kazazian HH Jr, Boeke JD (1996) Human L1 retrotransposon encodes a conserved endonuclease required for retrotransposition. *Cell* 87: 905–916
- Furtak V, Mulky A, Rawlings SA, Kozhaya L, Lee K, Kewalramani VN, Unutmaz D (2010) Perturbation of the P-body component Mov10 inhibits HIV-1 infectivity. *PLoS One* 5: e9081
- Garneau NL, Wilusz J, Wilusz CJ (2007) The highways and byways of mRNA decay. *Nat Rev Mol Cell Biol* 8: 113–126
- Gasior SL, Wakeman TP, Xu B, Deininger PL (2006) The human LINE-1 retrotransposon creates DNA double-strand breaks. *J Mol Biol* 357: 1383–1393
- Gilbert N, Lutz-Prigge S, Moran JV (2002) Genomic deletions created upon LINE-1 retrotransposition. *Cell* 110: 315–325
- Goodier JL (2016) Restricting retrotransposons: a review. *Mob DNA* 7: 16
- Goodier JL, Kazazian HH Jr (2008) Retrotransposons revisited: the restraint and rehabilitation of parasites. *Cell* 135: 23–35
- Goodier JL, Zhang L, Vetter MR, Kazazian HH Jr (2007) LINE-1 ORF1 protein localizes in stress granules with other RNA-binding proteins, including components of RNA interference RNA-induced silencing complex. *Mol Cell Biol* 27: 6469–6483
- Goodier JL, Cheung LE, Kazazian HH Jr (2012) MOV10 RNA helicase is a potent inhibitor of retrotransposition in cells. *PLoS Genet* 8: e1002941
- Goodier JL, Pereira GC, Cheung LE, Rose RJ, Kazazian HH Jr (2015) The broad-spectrum antiviral protein ZAP restricts human Retrotransposition. *PLoS Genet* 11: e1005252
- Gregersen LH, Schueler M, Munschauer M, Mastrobuoni G, Chen W, Kempa S, Dieterich C, Landthaler M (2014) MOV10 is a 5' to 3' RNA helicase contributing to UPF1 mRNA target degradation by translocation along 3' UTRs. *Mol Cell* 54: 573–585
- Han JS, Szak ST, Boeke JD (2004) Transcriptional disruption by the L1 retrotransposon and implications for mammalian transcriptomes. *Nature* 429: 268–274
- Haussecker D, Cao D, Huang Y, Parameswaran P, Fire AZ, Kay MA (2008) Capped small RNAs and MOV10 in human hepatitis delta virus replication. *Nat Struct Mol Biol* 15: 714–721
- Hu B, Ge X, Wang LF, Shi Z (2015a) Bat origin of human coronaviruses. *Virology* 12: 221
- Hu S, Li J, Xu F, Mei S, Le Duff Y, Yin L, Pang X, Cen S, Jin Q, Liang C et al (2015b) SAMHD1 inhibits LINE-1 Retrotransposition by promoting stress granule formation. *PLoS Genet* 11: e1005367
- Iskrow RC, McCabe MT, Mills RE, Torene S, Pittard WS, Neuwald AF, Van Meir EG, Vertino PM, Devine SE (2010) Natural mutagenesis of human genomes by endogenous retrotransposons. *Cell* 141: 1253–1261
- Kinomoto M, Kanno T, Shimura M, Ishizaka Y, Kojima A, Kurata T, Sata T, Tokunaga K (2007) All APOBEC3 family proteins differentially inhibit LINE-1 retrotransposition. *Nucleic Acids Res* 35: 2955–2964
- Lander ES, Linton LM, Birren B, Nusbaum C, Zody MC, Baldwin J, Devon K, Dewar K, Doyle M, FitzHugh W et al (2001) Initial sequencing and analysis of the human genome. *Nature* 409: 860–921
- Li X, Zhang J, Jia R, Cheng V, Xu X, Qiao W, Guo F, Liang C, Cen S (2013) The MOV10 helicase inhibits LINE-1 mobility. *J Biol Chem* 288: 21148–21160
- Liang W, Xu J, Yuan W, Song X, Zhang J, Wei W, Yu XF, Yang Y (2016) APOBEC3DE inhibits LINE-1 retrotransposition by interacting with ORF1p and influencing LINE reverse transcriptase activity. *PLoS One* 11: e0157220
- Lu C, Luo Z, Jager S, Krogan NJ, Peterlin BM (2012) Moloney leukemia virus type 10 inhibits reverse transcription and retrotransposition of intracisternal particles. *J Virol* 86: 10517–10523
- Luan DD, Korman MH, Jakubczak JL, Eickbush TH (1993) Reverse transcription of R2Bm RNA is primed by a nick at the chromosomal target site: a mechanism for non-LTR retrotransposition. *Cell* 72: 595–605
- Lykke-Andersen J, Wagner E (2005) Recruitment and activation of mRNA decay enzymes by two ARE-mediated decay activation domains in the proteins TTP and BRF-1. *Genes Dev* 19: 351–361
- MacDuff DA, Demorest ZL, Harris RS (2009) AID can restrict L1 retrotransposition suggesting a dual role in innate and adaptive immunity. *Nucleic Acids Res* 37: 1854–1867
- Moldovan JB, Moran JV (2015) The zinc-finger antiviral protein ZAP inhibits LINE and Alu Retrotransposition. *PLoS Genet* 11: e1005121
- Molliex A, Temirov J, Lee J, Coughlin M, Kanagaraj AP, Kim HJ, Mittag T, Taylor JP (2015) Phase separation by low complexity domains promotes stress granule assembly and drives pathological fibrillization. *Cell* 163: 123–133
- Mooslehner K, Muller U, Karls U, Hamann L, Harbers K (1991) Structure and expression of a gene encoding a putative GTP-binding protein identified by provirus integration in a transgenic mouse strain. *Mol Cell Biol* 11: 886–893
- Muckenfuss H, Hamdorf M, Held U, Perkovic M, Lower J, Cichutek K, Flory E, Schumann GG, Munk C (2006) APOBEC3 proteins inhibit human LINE-1 retrotransposition. *J Biol Chem* 281: 22161–22172
- Newton JC, Naik MT, Li GY, Murphy EL, Fawzi NL, Sedivy JM, Jogle G (2021) Phase separation of the LINE-1 ORF1 protein is mediated by the N-terminus and coiled-coil domain. *Biophys J* 120: 2181–2191
- Nott TJ, Petsalaki E, Farber P, Jervis D, Fussner E, Plochowitz A, Craggs TD, Bazett-Jones DP, Pawson T, Forman-Kay JD et al (2015) Phase transition of a disordered nuage protein generates environmentally responsive membraneless organelles. *Mol Cell* 57: 936–947
- Patel SS, Belmont BJ, Sante JM, Rexach MF (2007) Natively unfolded nucleoporins gate protein diffusion across the nuclear pore complex. *Cell* 129: 83–96
- Perez-Riverol Y, Bai J, Bandla C, Garcia-Seisdedos D, Hewapathirana S, Kamatchinathan S, Kundu DJ, Prakash A, Frericks-Zipper A, Eisenacher M et al (2022) The PRIDE database resources in 2022: a hub for mass spectrometry-based proteomics evidences. *Nucleic Acids Res* 50: D543–D552
- Puray-Chavez MN, Farghali MH, Yapo V, Huber AD, Liu D, Ndongwe TP, Casey MC, Laughlin TG, Hannink M, Tedbury PR et al (2019) Effects of Moloney leukemia virus 10 protein on hepatitis B virus infection and viral replication. *Viruses* 11: 651
- Ribbeck K, Gorlich D (2002) The permeability barrier of nuclear pore complexes appears to operate via hydrophobic exclusion. *EMBO J* 21: 2664–2671
- Richardson SR, Narvaiza I, Planegger RA, Weitzman MD, Moran JV (2014) APOBEC3A deaminates transiently exposed single-strand DNA during LINE-1 retrotransposition. *Elife* 3: e02008
- Schoenberg DR (2011) Mechanisms of endonuclease-mediated mRNA decay. *Wiley Interdiscip Rev RNA* 2: 582–600
- Schoggins JW, Wilson SJ, Panis M, Murphy MY, Jones CT, Bieniasz P, Rice CM (2011) A diverse range of gene products are effectors of the type I interferon antiviral response. *Nature* 472: 481–485

- Sheu-Gruttadauria J, MacRae IJ (2018) Phase transitions in the assembly and function of human miRISC. *Cell* 173: 946–957.e16
- Sil S, Boeke JD, Holt LJ (2022) Condensation of LINE-1 is required for retrotransposition. *bioRxiv* <https://doi.org/10.1101/2022.04.11.487880> [PREPRINT]
- Skariah G, Seimetz J, Norsworthy M, Lannom MC, Kenny PJ, Elrakhawy M, Forsthoefel C, Drnevich J, Kalsotra A, Ceman S (2017) Mov10 suppresses retroelements and regulates neuronal development and function in the developing brain. *BMC Biol* 15: 54
- Stenglein MD, Harris RS (2006) APOBEC3B and APOBEC3F inhibit L1 retrotransposition by a DNA deamination-independent mechanism. *J Biol Chem* 281: 16837–16841
- Tan L, Sarkis PT, Wang T, Tian C, Yu XF (2009) Sole copy of Z2-type human cytidine deaminase APOBEC3H has inhibitory activity against retrotransposons and HIV-1. *FASEB J* 23: 279–287
- Taylor MS, Altukhov I (2018) Dissection of affinity captured LINE-1 macromolecular complexes. *Elife* 7: e30094
- Taylor MS, LaCava J, Mita P, Molloy KR, Huang CR, Li D, Adney EM, Jiang H, Burns KH, Chait BT et al (2013) Affinity proteomics reveals human host factors implicated in discrete stages of LINE-1 retrotransposition. *Cell* 155: 1034–1048
- Taylor JP, Brown RH Jr, Cleveland DW (2016) Decoding ALS: from genes to mechanism. *Nature* 539: 197–206
- Wang Z, Jiao X, Carr-Schmid A, Kiledjian M (2002) The hDcp2 protein is a mammalian mRNA decapping enzyme. *Proc Natl Acad Sci USA* 99: 12663–12668
- Wang X, Han Y, Dang Y, Fu W, Zhou T, Ptak RC, Zheng YH (2010) Moloney leukemia virus 10 (MOV10) protein inhibits retrovirus replication. *J Biol Chem* 285: 14346–14355
- Wang H, Chang L, Wang X, Su A, Feng C, Fu Y, Chen D, Zheng N, Wu Z (2016) MOV10 interacts with enterovirus 71 genomic 5'UTR and modulates viral replication. *Biochem Biophys Res Commun* 479: 571–577
- Warkocki Z, Krawczyk PS, Adamska D, Bijata K, Garcia-Perez JL, Dziembowski A (2018) Uridylation by TUT4/7 restricts retrotransposition of human LINE-1s. *Cell* 174: 1537–1548.e29
- Weber SC, Brangwynne CP (2015) Inverse size scaling of the nucleolus by a concentration-dependent phase transition. *Curr Biol* 25: 641–646
- Wippich F, Bodenmiller B, Trajkovska MC, Wanka S, Aebersold R, Pelkmans L (2013) Dual specificity kinase DYRK3 couples stress granule condensation/dissolution to mTORC1 signaling. *Cell* 152: 791–805
- Woodruff JB, Ferreira Gomes B, Widlund PO, Mahamid J, Honigsmann A, Hyman AA (2017) The centrosome is a selective condensate that nucleates microtubules by concentrating tubulin. *Cell* 169: 1066–1077.e10
- Zhang J, Huang F, Tan L, Bai C, Chen B, Liu J, Liang J, Liu C, Zhang S, Lu G et al (2016) Host protein Moloney leukemia virus 10 (MOV10) acts as a restriction factor of influenza A virus by inhibiting the nuclear import of the viral nucleoprotein. *J Virol* 90: 3966–3980